AGU PUBLICATIONS

JGR

Journal of Geophysical Research: Atmospheres

RESEARCH ARTICLE

10.1002/2017JD027976

Key Points:
- An extensive and expanded data set of oxygenated VOCs in ambient air in the Los Angeles basin is analyzed
- The composition of directly emitted oxygenated VOCs is determined after accounting for the effects of their chemical formation and removal
- Aldehydes are important for urban photochemistry, but their sources remain poorly understood

Supporting Information:
- Supporting Information S1

Correspondence to:
J. A. de Gouw,
joost.degouw@colorado.edu

Citation:
de Gouw, J. A., Gilman, J. B., Kim, S.-W., Alvarez, S. L., Dusanter, S., Graus, M., et al. (2018). Chemistry of volatile organic compounds in the Los Angeles Basin: Formation of oxygenated compounds and determination of emission ratios. *Journal of Geophysical Research: Atmospheres*, *123*, 2298–2319. https://doi.org/10.1002/2017JD027976

Received 30 OCT 2017
Accepted 25 JAN 2018
Accepted article online 6 FEB 2018
Published online 22 FEB 2018

Chemistry of Volatile Organic Compounds in the Los Angeles Basin: Formation of Oxygenated Compounds and Determination of Emission Ratios

J. A. de Gouw[1,2,3], J. B. Gilman[2], S.-W. Kim[1,2], S. L. Alvarez[4], S. Dusanter[5], M. Graus[1,2,6], S. M. Griffith[7], G. Isaacman-VanWertz[8], W. C. Kuster[2], B. L. Lefer[4,9], B. M. Lerner[1,2,10], B. C. McDonald[1,2], B. Rappenglück[4], J. M. Roberts[2], P. S. Stevens[11], J. Stutz[12], R. Thalman[13], P. R. Veres[1,2], R. Volkamer[1,3], C. Warneke[1,2], R. A. Washenfelder[2], and C. J. Young[1,2,14]

[1]Cooperative Institute for Research in Environmental Sciences, University of Colorado, Boulder, CO, USA, [2]Earth System Research Laboratory, National Oceanic and Atmospheric Administration, Boulder, CO, USA, [3]Department of Chemistry and Biochemistry, University of Colorado, Boulder, CO, USA, [4]Department of Earth and Atmospheric Sciences, University of Houston, Houston, TX, USA, [5]IMT Lille Douai, SAGE, Département Sciences de l'Atmosphère et Génie de l'Environnement, University Lille, Lille, France, [6]Now at Institute of Atmospheric and Cryospheric Sciences, University of Innsbruck, Innsbruck, Austria, [7]Department of Chemistry, Hong Kong University of Science and Technology, Clear Water Bay, Hong Kong, [8]Department of Civil and Environmental Engineering, Virginia Polytechnic Institute and State University, Blacksburg, VA, USA, [9]Now at NASA Earth Science Division, Washington, DC, USA, [10]Now at Aerodyne Research, Billerica, MA, USA, [11]School of Public and Environmental Affairs, Indiana University, Bloomington, IN, USA, [12]Department of Atmospheric and Oceanic Sciences, University of California, Los Angeles, CA, USA, [13]Department of Chemistry, Snow College, Richfield, UT, USA, [14]Now at Department of Chemistry, York University, Toronto, Canada

Abstract We analyze an expanded data set of oxygenated volatile organic compounds (OVOCs) in air measured by several instruments at a surface site in Pasadena near Los Angeles during the National Oceanic and Atmospheric Administration California Nexus study in 2010. The contributions of emissions, chemical formation, and removal are quantified for each OVOC using CO as a tracer of emissions and the OH exposure of the sampled air masses calculated from hydrocarbon ratios. The method for separating emissions from chemical formation is evaluated using output for Pasadena from the Weather Research and Forecasting-Chemistry model. The model is analyzed by the same method as the measurement data, and the emission ratios versus CO calculated from the model output agree for ketones with the inventory used in the model but overestimate aldehydes by ~70%. In contrast with the measurements, nighttime formation of OVOCs is significant in the model and is attributed to overestimated precursor emissions and overestimated rate coefficients for the reactions of the precursors with ozone and NO_3. Most measured aldehydes correlated strongly with CO at night, suggesting a contribution from motor vehicle emissions. However, the emission ratios of most aldehydes versus CO are higher than those reported in motor vehicle emissions and the aldehyde sources remain unclear. Formation of several OVOCs is investigated in terms of the removal of specific precursors. Direct emissions of alcohols and aldehydes contribute significantly to OH reactivity throughout the day, and these emissions should be accurately represented in models describing ozone formation.

Plain Language Summary We report new measurements of volatile organic compounds (VOCs) in ambient air in the Los Angeles basin. Chemical reactions between VOCs and nitrogen oxides form ozone and fine particles, two important pollutants in Los Angeles smog. It is therefore important to understand VOC emission sources. In this work, we derive the composition of VOC emissions using ambient measurements at Pasadena in 2010. The study is complicated due to rapid chemical reactions that can form and remove VOCs in between the time of emission and measurement. After correcting for this chemistry, it is shown that emissions of many oxygen-containing VOCs are important for the formation of ozone.

1. Introduction

The emissions of volatile organic compounds (VOCs) and their photooxidation in the presence of nitrogen oxides (NO_x) may lead to the formation of secondary pollutants such as ozone (Carter, 1994; Derwent et al., 1996) and secondary organic aerosol (Odum et al., 1997). To understand these processes in detail,

it is essential to accurately describe anthropogenic VOC emissions and photochemical processing. Determining emissions is particularly challenging for oxygenated VOCs (OVOCs), which have many sources including fossil-fuel combustion, vegetation and biomass burning, and the use of volatile chemical products (cleaning agents, coatings, pesticides, personal care products, etc), and which can also be formed in the atmosphere from the oxidation of precursors. Despite these complications, it is important to understand the sources of OVOCs in detail. Carbonyls can be photolyzed and provide a direct source of radicals (Griffith et al., 2016; Lee et al., 1998). OVOCs like alcohols and aldehydes are reactive themselves and can provide a significant fraction of reactivity with hydroxyl radicals in urban air (Goldan et al., 2004). Carbonyls are also important precursors of peroxyacyl nitrates, which can sequester NO_x from air masses and provide a transport mechanism for NO_x to more remote regions of the atmosphere (Roberts, 1990).

Motor vehicle emissions of OVOCs have been determined from dynamometer and tunnel studies (Gentner et al., 2013; Kirchstetter, Singer, Harley, Kendall, & Hesson, 1999; Kirchstetter, Singer, Harley, Kendall, & Traverse, 1999; Legreid, Reimann, et al., 2007; May et al., 2014; Schauer et al., 2002). Determining OVOC emissions from ambient measurements is more complicated as most air masses in large metropolitan areas contain a mixture of emissions from nearby sources and aged emissions from sources further away. Reactive OVOCs can therefore be partially removed and/or chemically formed in between the time of emission and sampling. Separating the contributions from direct emissions and chemical formation has been attempted in various ways. Observations at night and during the early-morning rush hour are the most strongly impacted by direct emissions and have been used to derive emission ratios between OVOCs and inert combustion tracers (Borbon et al., 2013; Parrish et al., 2012; Warneke et al., 2007). Statistical analyses like principal component analysis, positive matrix factorization, chemical mass balance, and others are widely used for source attribution of VOCs (Cai et al., 2010; Guo et al., 2004; Jorquera & Rappenglück, 2004; Leuchner & Rappenglück, 2010; Song et al., 2007). An important limitation of these methods, however, is that they do not explicitly account for chemical removal and formation and will typically attribute the more aged air masses in a data set to a separate source (Bon et al., 2011; Yuan et al., 2012). Seasonal cycles and correlation with carbon monoxide can be useful to discern the effects of direct emission in the winter, and secondary formation and biogenic sources in the summer (Legreid, Balzani Loov, et al., 2007). Emissions themselves can be seasonally dependent; however, residential wood burning, for example, can be an additional source of OVOCs in the wintertime.

The CalNex study in 2010 provided an extensive data set of VOCs, including many oxygenated species, at an urban site in Pasadena in the Los Angeles basin in May–June of 2010. OVOC data from CalNex have been analyzed and presented in several other publications. Measurements of glyoxal were explained in terms of secondary formation from aromatic VOCs, isoprene, and ethyne (Washenfelder et al., 2011). Measurements of organic acids revealed efficient secondary formation (Veres et al., 2011), which could not be fully explained by the measured precursors and known formation mechanisms (Yuan et al., 2015). Enhancement ratios of ethanol were found to be much higher than in earlier urban studies, which were partially attributed to an increase in fuel ethanol use in 2010 (de Gouw et al., 2012). Measurements of 11 different aldehydes, ketones, and alcohols made by gas chromatography-mass spectrometry (GC-MS) were used to determine emission ratios of these compounds (Borbon et al., 2013). The differences in VOC emissions and chemistry between weekends and weekdays were studied and revealed faster removal of hydrocarbons on weekends when NO_x emissions were lower (Warneke et al., 2013).

Since our earlier analysis of the GC-MS data set (Borbon et al., 2013), the development of new peak fitting software (Isaacman-VanWertz et al., 2017) has enabled the quantification of several more compounds from this data set. New measurement data for hydrocarbons were analyzed in a companion paper with a focus on the determination of emission ratios (de Gouw et al., 2017). It was found that nighttime chemical removal of alkenes needs to be accounted for to get accurate emission ratios. Also, output from the chemistry-transport model WRF-Chem was used to evaluate the analysis methods. In this work, we analyze the new data for OVOCs obtained from the GC-MS data set with a focus on determining emission ratios of OVOCs and describing the secondary formation of these compounds. The new data are analyzed in combination with the existing OVOC data including those from other instruments.

After summarizing the data set as a whole, we describe the removal of the measured compounds by OH and by photolysis. We use these removal rates in describing the measured OVOCs as a function of OH exposure, which

was calculated from hydrocarbon ratios as described in detail in our companion paper (de Gouw et al., 2017). This allows the contributions from direct emissions and photochemical formation to be separated. Nighttime formation is studied by describing the measured OVOCs as a function of ozone exposure. The data analysis method used to separate emissions from chemical formation is evaluated using output from the chemistry-transport model WRF-Chem. The calculated OVOC emission ratios are compared with other studies in the literature. Finally, we discuss the implications of these findings for atmospheric chemistry in urban atmospheres.

2. Measurements and Data Description

2.1. Measurement Location and Meteorology

The measurement site and meteorology were discussed in our companion paper (de Gouw et al., 2017). Briefly, the study took place on the campus of the California Institute of Technology in Pasadena from 15 May through 15 June 2010. During the day, the sampled air masses came from the western part of the Los Angeles basin transporting emissions from downtown Los Angeles to the site. At night, winds were calm, and the sampled air masses contained emissions from the area centered on Pasadena.

2.2. VOC Measurements

Volatile organic compound data from seven different instruments are used in this work:

1. A large set of alkanes, alkenes, aromatics, and OVOCs was measured using a two-channel in situ GC-MS (Borbon et al., 2013; de Gouw et al., 2017; Gilman et al., 2010; Goldan et al., 2004).
2. A subset of the species measured by GC-MS was monitored with higher time resolution by proton-transfer ion trap mass spectrometry (Warneke et al., 2005).
3. Formaldehyde was measured by a Hantzsch monitor (Hak et al., 2005; Warneke et al., 2011).
4. Formaldehyde was also determined using a long-path differential optical absorption spectroscopy (LP-DOAS) measurement. The instrument was located on top of the Millikan library, which is approximately 550 m from the main site and 33 m higher in elevation. Four retroreflectors were placed in the San Gabriel mountains at elevations that were 78, 121, 255, and 556 m above the reference ground level at Caltech (Tsai et al., 2014; Warneke et al., 2011).
5. Gas-phase organic acids were measured using acetate-ion chemical ionization mass spectrometry (Veres et al., 2011). The instrument was described in more detail elsewhere, and the formic acid measurements were compared with those from two other instruments (Veres et al., 2008). During CalNex, instrument backgrounds were determined by passing the sample air through a sodium carbonate denuder and subtracted from the ambient data. This method of background subtraction was determined to be 98 ± 6% effective.
6. Glyoxal was measured using an incoherent broadband cavity-enhanced absorption spectroscopy instrument (Washenfelder et al., 2011).
7. Glyoxal was also measured using a cavity-enhanced DOAS instrument that was operated on top of the Millikan library (Thalman & Volkamer, 2010).

The times that the different measurements were operational are shown in Figure S1 in the supporting information. The GC-MS took one 5 min sample every 30 min. Unless otherwise noted, the other measurements are averaged onto the sampling times of the GC-MS for this analysis.

Additional measurements used in this analysis included those of carbon monoxide (CO) by vacuum ultraviolet resonance fluorescence (Gerbig et al., 1999), ozone by NO chemiluminescence, OH radicals by laser-induced fluorescence (Griffith et al., 2016), and NO_3 radicals by LP-DOAS (Tsai et al., 2014). The latter measurement was made by the same LP-DOAS instrument as used for formaldehyde. Photolysis rates of NO_2 were measured by scanning actinic flux spectroradiometry (Shetter & Mueller, 1999).

2.3. WRF-Chem Model

Output from the Weather Research and Forecasting-Chemistry (WRF-Chem) model is used to evaluate our data analysis method that separates the contributions from direct emissions and chemical formation of the OVOCs. The model setup and performance have been described previously (Kim et al., 2016), and the specific model run used in this analysis was described in our companion paper (de Gouw et al., 2017). Briefly, we use version 3.4.1 of WRF-Chem (Grell et al., 2005), and the model is run for the State of California at 4×4 km^2

Table 1
Calculated Emission Ratios (ER_{OVOC}) and Their Error Estimates (ΔER_{OVOC}) of the Measured Oxygenated Volatile Organic Compounds (VOCs) Versus Carbon Monoxide Determined From Fits of Equation (6) to the Measurements

Compound	k_{OH} @ 298 K		ER_{OVOC}	ΔER_{OVOC}	Background	r^2
	cm^3 $molecule^{-1}$ s^{-1}	Reference	pptv [ppbv CO]$^{-1}$		pptv	
Formaldehyde	9.37×10^{-12}	(Atkinson & Arey, 2003)	1.3	1.3	530 ± 30	0.823
Acetaldehyde	1.5×10^{-11}	(Atkinson & Arey, 2003)	4.3	0.8	150 ± 20	0.870
Propanal	2.0×10^{-11}	(Atkinson & Arey, 2003)	1.00	0.12	78 ± 5	0.828
Butanal	2.4×10^{-11}	(Atkinson & Arey, 2003)	0.23	0.02	27.2 ± 1.1	0.752
2-Methylpropanal	2.6×10^{-11}	(Atkinson & Arey, 2003)	0.152	0.007	6.2 ± 0.6	0.772
Hexanal	3.0×10^{-11}	(Atkinson & Arey, 2003)	0.57	0.06	75 ± 2	0.592
Acrolein	1.96×10^{-11}	(Atkinson, 1986)	1.40	0.03	14 ± 3	0.856
Benzaldehyde	1.2×10^{-11}	(Atkinson & Arey, 2003)	0.89	0.05	0[a]	0.709
Acetone	1.7×10^{-13}	(Atkinson & Arey, 2003)	11.6	1.1	870 ± 90	0.615
Methylethylketone	1.22×10^{-12}	(Atkinson & Arey, 2003)	0.88	0.15	0 ± 8	0.719
Methanol	9.4×10^{-13}	(Atkinson & Arey, 2003)	21.2	1.4	3200 ± 300	0.156
Ethanol	3.2×10^{-12}	(Atkinson & Arey, 2003)	45.7	1.0	800 ± 200	0.624
n-Propanol	5.8×10^{-12}	(Atkinson & Arey, 2003)	0.32	0.02	25 ± 4	0.135
i-Propanol	5.1×10^{-12}	(Atkinson & Arey, 2003)	9.9	0.3	140 ± 50	0.553
Formic acid	4.5×10^{-13}	(Atkinson et al., 1997)	1.2	0.8	880 ± 40	0.704
Propionic acid	1.2×10^{-12}	(Atkinson et al., 1997)	3.1	1.2	0[a]	0.569
Acrylic acid	1.75×10^{-11}	(Teruel et al., 2007)	0.05	0.02	0[a]	0.562
Methacrylic acid	1.75×10^{-11}[b]		0.22	0.05	0[a]	0.208
Pyruvic acid	1.24×10^{-13}	(Mellouki & Mu, 2003)	0.06	0.03	0[a]	0.670
Methylformate	1.83×10^{-13}	(Szilagyi et al., 2004)	0.14	0.03	53.4 ± 1.3	0.808
Methylacetate	3.45×10^{-13}	(El Boudali et al., 1996)	0.228	0.012	13 ± 2	0.357
Glyoxal	1.1×10^{-11}	(Atkinson & Arey, 2003)	0.17	0.06	0[a]	0.699
3-Furaldehyde	4.85×10^{-11}	(Bierbach et al., 1995)	0.125	0.008	0.6 ± 0.8	0.503
2,3-Butadione	2.48×10^{-13}	(Dagaut et al., 1988)	0.125	0.004	8.9 ± 0.6	0.604
Isocyanic acid	1×10^{-15}	(Roberts et al., 2011)	0.025	0.012	9.0 ± 0.6	0.684
Nitromethane	1.58×10^{-14}	(Liu et al., 1990)	0.047	0.005	0.5 ± 0.3	0.815

Note. Also shown are the rate coefficients for the reaction with OH that are needed in the fits, the background mixing ratios determined from the fits, and the values of the linear correlation coefficient, r^2, for the fitted versus measured mixing ratios.
[a]Set to zero as fit returned negative value. [b]Assumed the same rate coefficient as for acrylic acid.

horizontal resolution. The model uses NO_x and CO emissions from a fuel-based inventory for motor-vehicle emissions (McDonald et al., 2012, 2013, 2014). Emissions of anthropogenic VOCs are taken from the 2011 National Emissions Inventory (Ahmadov et al., 2015). The Biogenic Emissions Inventory System version 3.13 is used, and emissions from urban vegetation are added (Scott & Benjamin, 2003). The Regional Atmospheric Chemistry Mechanism (RACM) (Stockwell et al., 1997) is used, with updated reaction rate coefficients (Kim et al., 2009).

2.4. Rate Coefficients and Photolysis Rates

Rate coefficients for the reactions between OVOCs and OH are used throughout this manuscript and are given in Table 1. We use the rate coefficients at 298 K, as a single value is needed in the analysis and 298 K was close to the average daytime high. Reactions with ozone and NO_3 are inefficient for all measured OVOCs (Atkinson, 1991; Atkinson & Arey, 2003; Al Mulla et al., 2010; Bernard et al., 2013) except for 3-furaldehyde, which reacts efficiently with NO_3 (Colmenar et al., 2012). Rate coefficients for the reactions of the unsaturated OVOCs studied here with ozone and NO_3 are given in Table S1 in the supporting information.

Clear-sky photolysis rates for different compounds are calculated in this work from the parameterization used in the Master Chemical Mechanism v3.3.1 (Saunders et al., 2003):

$$\text{clear sky } j = l(\cos\chi)^m \exp(-n.\sec\chi) \quad (1)$$

where χ is the solar zenith angle and l, m, and n are parameters listed for different photolysis rates. Only j_{NO2} photolysis rates were reported from the radiometer measurements at the site. To estimate photolysis rates for OVOCs, we use the following equation:

$$j_{OVOC} = \text{clear sky } j_{OVOC} \times \frac{\text{measured } j_{NO2}}{\text{clear sky } j_{NO2}} \quad (2)$$

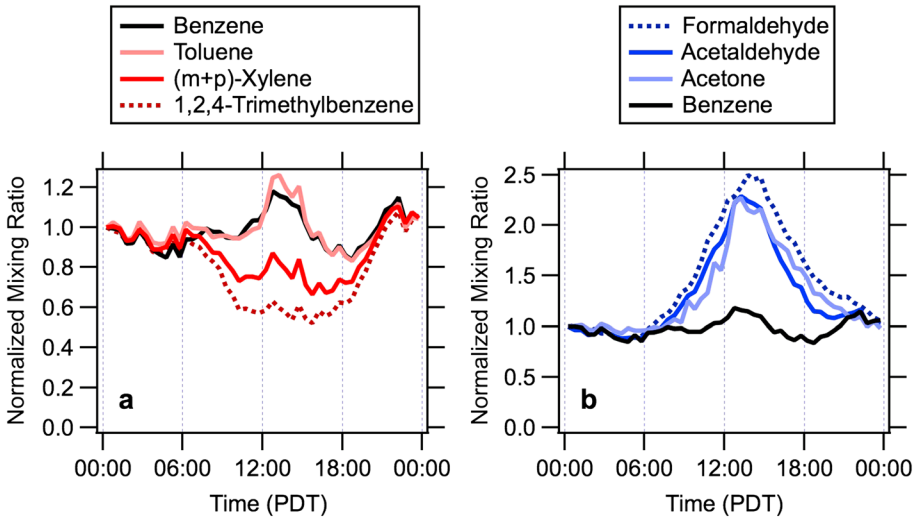

Figure 1. Average diurnal variations of selected (a) aromatics and (b) oxygenated volatile organic compounds. The data are averaged in 30 min bins and normalized to a midnight value of 1 for comparison between the different measurements.

In other words, we assume that the photolysis rates for all OVOCs are reduced relative to their clear-sky rates by the same factor as for j_{NO2}.

3. Results and Discussion

3.1. Formation, Emission, and Removal of OVOCs

Evidence for the daytime removal of hydrocarbons and formation of OVOCs is readily observed from the average diurnal variations of different compounds. Figure 1 shows the diurnal variations of a few selected hydrocarbons and OVOCs. The data are all normalized to a midnight value of 1 for ease of comparison. Figure 1a shows that the more reactive a hydrocarbon ((m + p)-xylenes, 1,2,4-trimethylbenzene) with respect to OH, the more it was removed during the daytime relative to the less reactive compounds (benzene and toluene). In our companion paper, we show that this was true for all hydrocarbons that are primarily removed by OH (alkanes, small alkenes, and aromatics), but not for alkenes that react efficiently with ozone and/or NO_3 (de Gouw et al., 2017). In contrast, many OVOCs showed enhancements during the daytime, as they were chemically formed (Figure 1b).

Average daytime (10:00–18:00 Pacific Daylight Time) and nighttime (22:00–6:00 Pacific Daylight Time) mixing ratios of the OVOCs studied in this paper are presented in Figure 2a. The highest mixing ratios were observed for three alcohols (ethanol, methanol, and i-propanol), a ketone (acetone), two aldehydes (formaldehyde and acetaldehyde), and two acids (formic and propionic acid). Mixing ratios of several aldehydes, ketones, and acids were significantly higher during the day relative to the night because of photochemical formation. Alcohols had lower averages during the day relative to the night; these compounds do not have strong photochemical sources. Mixing ratios of methacrolein and methylvinylketone, two oxidation products from isoprene oxidation, were also significantly enhanced during the day.

A different way to visualize the effects of chemistry on VOC concentrations is through the use of species-to-species scatterplots; some examples are given in Figure S2. The daytime formation of OVOCs limits the degree of correlation between OVOCs and CO. However, the correlation between several OVOCs and CO was strong for the nighttime data only (Figures 2b and S2). Four aldehydes (acetaldehyde, propanal, butanal, and acrolein) correlated with CO with an $r^2 > 0.8$. Such high values of r^2 were otherwise only observed for aromatic hydrocarbons (de Gouw et al., 2017) and suggest that direct emissions from motor vehicles are a source of these compounds. Four organic acids did not correlate with CO at night ($r^2 < 0.15$). Acrylic, methacrylic, and pyruvic acid were close to their respective detection limits at night, which limits the degree of correlation. Nevertheless, the different organic acids correlated more strongly with each other at night (Figure S3), and we hypothesize that this correlation is caused by deposition, which provides a common

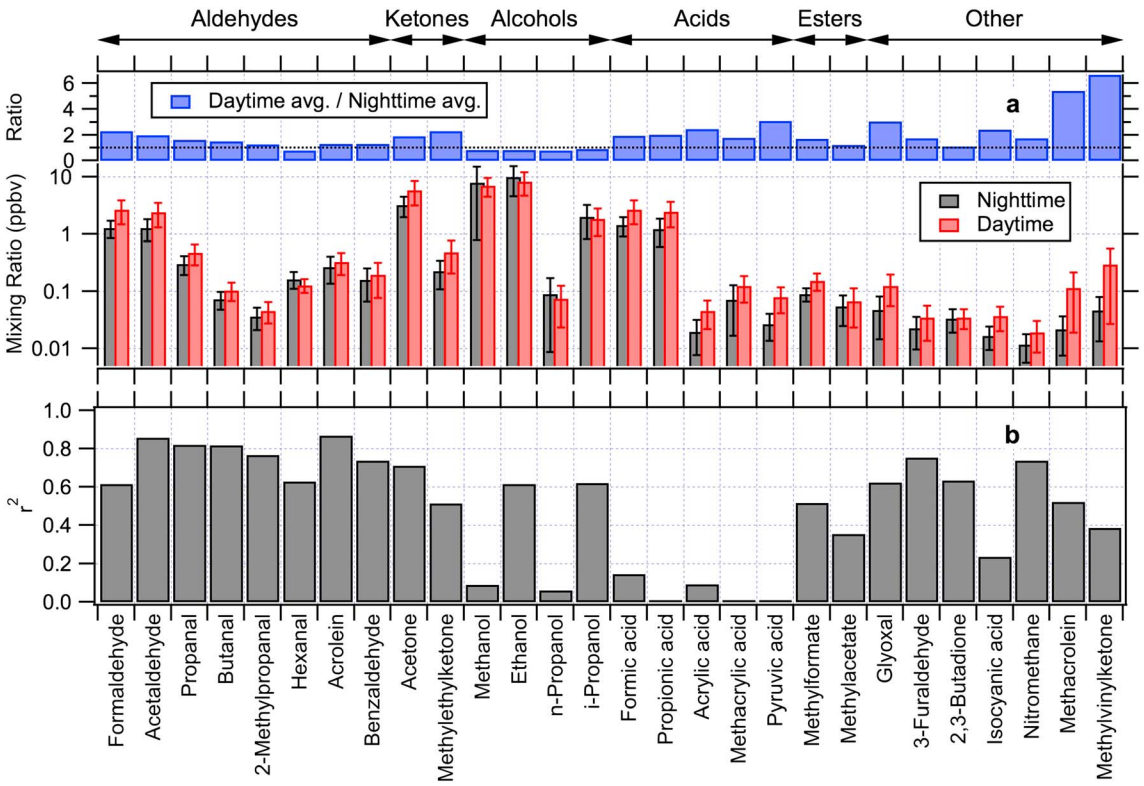

Figure 2. (a) Average mixing ratios for the different oxygenated volatile organic compounds (OVOCs) studied here. Nighttime (22:00–6:00 Pacific Daylight Time) averages are shown in black and daytime (10:00–18:00 Pacific Daylight Time) averages in red with the error bars indicating the standard deviations. The ratio between daytime and nighttime averages is shown in the upper panel in blue. The dotted line shows a ratio of 1. (b) Linear correlation coefficients between nighttime data for the measured OVOCs with CO.

nighttime loss process that can be efficient for formic acid (Brophy & Farmer, 2015), and which decouples the organic acids from CO. The nighttime data for 11 different OVOCs (3 alcohols, 5 aldehydes, and 3 ketones) were used in a previous publication to determine emission ratios versus CO (Borbon et al., 2013).

Several of the OVOCs measured in this study are very reactive with OH, and their removal during the day needs to be accounted for in separating their contributions from emissions and photochemical formation. In addition, some carbonyls can be photolyzed efficiently, which provides an additional loss process to OH chemistry. The concentrations of OH radicals were measured at the site, and the average diurnal variation is shown in Figure 3a. The average loss rate for different OVOCs versus reaction with OH can be calculated by multiplying their OH rate coefficients with the diurnally averaged OH concentrations. The results are shown for four selected OVOCs in Figures 3c–3f. Reactions with ozone and NO_3 are not efficient for all of the OVOCs studied here except for 3-furaldehyde (Colmenar et al., 2012) (Table S1).

The average diurnal variation in measured and clear-sky NO_2 photolysis rates are shown in Figure 3b. In general, the clear-sky j_{NO2} is somewhat higher than the average measured j_{NO2} plus 1 times its standard deviation. The difference was largest in the morning when fog was sometimes present at the site. Photolysis rates for OVOCs are calculated using equations (1) and (2) (Figures 3c–3f) and compared with the OH reaction loss rates. Figure S3 compares the average daytime photolysis and OH reaction loss rates for all measured OVOCs. For formaldehyde, glyoxal, and 2,3-butadione, the photolysis rates were higher than the OH loss rates. For most other carbonyls, the photolysis rates were lower, though not negligible, compared with the OH loss rates.

3.2. Determination of Oxygenated VOC Emission Ratios

In our companion paper, we described how the degree of chemical processing of the sampled air masses could be quantified using measured hydrocarbon ratios (de Gouw et al., 2017). Briefly, the analysis

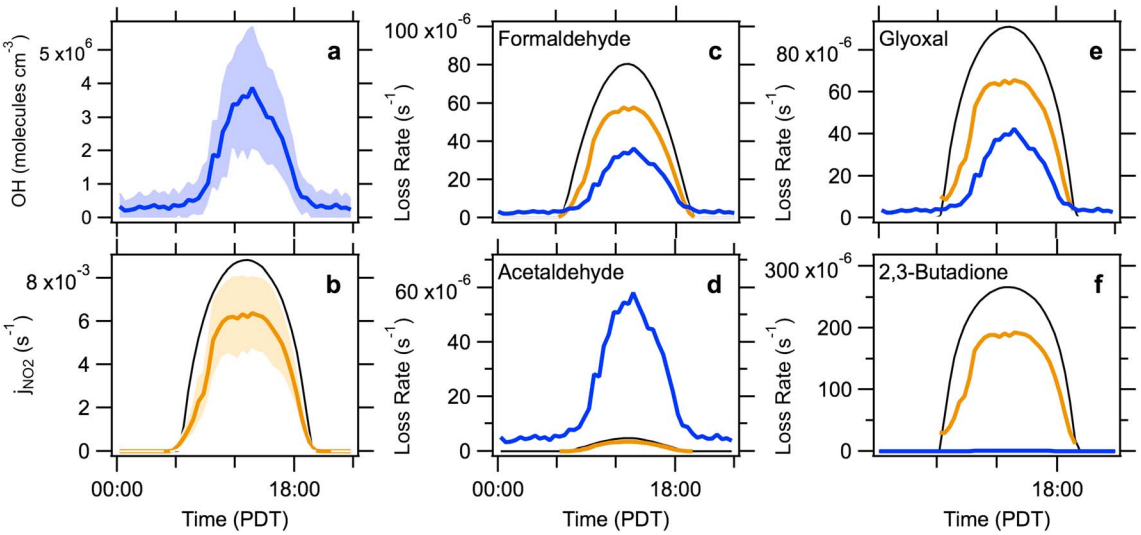

Figure 3. Average diurnal variations of (a) OH and (b) j_{NO2}, with the solid curves representing the average in 30 min bins and the shaded areas representing the 1-σ variability. The black line in panel b shows the clear-sky j_{NO2} photolysis rate for the latitude and time of the measurements calculated using equation (1). (c–f) Calculated loss rates for four selected carbonyls versus OH in blue and versus photolysis in mustard, with the black lines showing the clear-sky photolysis rates.

assumes that different hydrocarbons are emitted with the same composition across the basin but are removed at different rates dictated by their reaction rate coefficients with OH (or ozone for nighttime processing). Measured ratios of benzene versus 1,2,4-trimethylbenzene were used to define an OH exposure, that is, the time-integrated exposure of the sampled emissions to OH radicals. For nighttime data only, measured ratios of benzene versus cis-2-butene were used to define an ozone exposure (time-integrated exposure of the sampled emissions to ozone). For more details we refer the reader to our companion paper (de Gouw et al., 2017). This same framework will be used here to describe the OVOC observations.

Assuming the following set of chemical reactions:

$$\mathrm{HC} + \mathrm{OH} \xrightarrow{k_{\mathrm{HC}}} \mathrm{OVOC} \tag{3a}$$

$$\mathrm{OVOC} + \mathrm{OH} \xrightarrow{k_{\mathrm{OVOC}}} \text{products} \tag{3b}$$

$$\mathrm{OVOC} + h\nu \xrightarrow{j_{\mathrm{OVOC}}} \text{products} \tag{3c}$$

We can write down the kinetic equations for precursor hydrocarbon HC and OVOC as follows:

$$\frac{d[\mathrm{HC}]}{dt} = -k_{\mathrm{HC}}[\mathrm{OH}][\mathrm{HC}] \tag{4a}$$

$$\frac{d[\mathrm{OVOC}]}{dt} = -(k_{\mathrm{OVOC}}[\mathrm{OH}] + j_{\mathrm{OVOC}})[\mathrm{OVOC}] + k_{\mathrm{HC}}[\mathrm{OH}][\mathrm{HC}] \tag{4b}$$

Because the changes in the sampled air masses are expressed here as a function of OH exposure (and not photon exposure), the loss by photolysis is approximated by assuming an increased OH reaction rate coefficient for the OVOCs. In equation (4b), the total OVOC loss ($k_{\mathrm{OVOC}}[\mathrm{OH}] + j_{\mathrm{OVOC}}$) is replaced by $k^*_{\mathrm{OVOC}}[\mathrm{OH}]$, where the effective rate coefficient k^*_{OVOC} is calculated from k_{OVOC} plus the average additional loss by photolysis shown in Figure S3. With this approximation, the analytical solutions of equations (4a) and (4b) are

$$[\mathrm{HC}] = [\mathrm{HC}]_0 \times e^{-k_{\mathrm{HC}}[\mathrm{OH}]\Delta t} \tag{5a}$$

$$[\mathrm{OVOC}] = [\mathrm{OVOC}]_0 \times e^{-k^*_{\mathrm{OVOC}}[\mathrm{OH}]\Delta t} + [\mathrm{HC}]_0 \times \frac{k_{\mathrm{HC}}}{k^*_{\mathrm{OVOC}} - k_{\mathrm{HC}}} \times \left(e^{-k_{\mathrm{HC}}[\mathrm{OH}]\Delta t} - e^{-k^*_{\mathrm{OVOC}}[\mathrm{OH}]\Delta t}\right) \tag{5b}$$

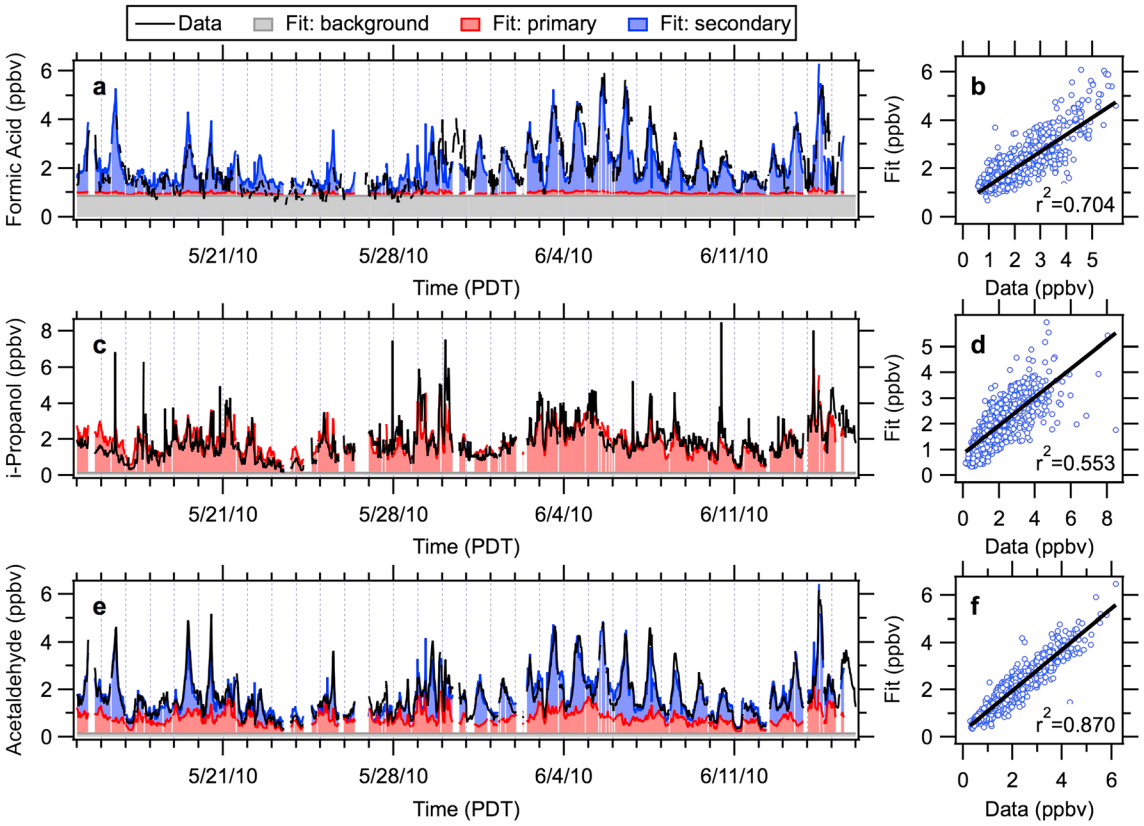

Figure 4. Examples of a fit of equation (6) to the data for three selected oxygenated volatile organic compounds: (a and b) formic acid, (c and d) i-propanol, and (e and f) acetaldehyde. (left column) Entire time series; (right column) scatterplots of the fit results versus the measured data.

The first term in equation (5b) represents the direct emission of OVOC and its removal in time. The second term represents the chemical formation of OVOC from its precursor hydrocarbon HC. To account for transport and mixing, we look at the ratio of OVOCs relative to CO, and we can write:

$$\begin{aligned}\mathrm{OVOC} = \mathrm{background} + \mathrm{ER_{OVOC}} \times \Delta\mathrm{CO} \times e^{-\left(k^*_{\mathrm{OVOC}} - k_{\mathrm{CO}}\right)[\mathrm{OH}]\Delta t} \\ + \mathrm{ER_{HC}} \times \Delta\mathrm{CO} \times \frac{k_{\mathrm{HC}}}{k^*_{\mathrm{OVOC}} - k_{\mathrm{HC}}} \times \left(e^{-\left(k_{\mathrm{HC}} - k_{\mathrm{CO}}\right)[\mathrm{OH}]\Delta t} - e^{-\left(k^*_{\mathrm{OVOC}} - k_{\mathrm{CO}}\right)[\mathrm{OH}]\Delta t}\right)\end{aligned} \tag{6}$$

In this equation, $\mathrm{ER_{OVOC}}$ and $\mathrm{ER_{HC}}$ are the emission ratios versus CO of the OVOC and HC, respectively, ΔCO is the excess CO mixing ratio over its background, k_{CO} is the OH reaction rate coefficient for CO, and background is the background mixing ratio of the OVOC. A single value of the CO background of 115 ± 10 ppbv was determined from the intercepts of scatterplots of reactive hydrocarbons versus CO, as described in our companion paper (de Gouw et al., 2017). As mentioned above, the OH exposure, $[\mathrm{OH}]\Delta t$, is calculated from the ratio between the measured benzene and 1,2,4-trimethylbenzene concentrations, which was described in detail in our companion paper (de Gouw et al., 2017), and not from the measured OH concentrations at the site. The analysis, therefore, does not assume that the sampled air masses had the same OH concentrations and photolysis rates during transport as observed at the site. The only assumption is that the relative importance of photolysis and OH removal was the same during transport as calculated at the site (Figures 3 and S4).

Equation (6) was fit to the measured time series of all OVOCs. The excess CO (ΔCO) and OH exposure ($[\mathrm{OH}]\Delta t$) are taken from the measurements and thus different for each sample time. The rate coefficient k^*_{OVOC} is a constant representing the combined loss to OH and photolysis as discussed above. The four free parameters in the fits are (1) the OVOC background, (2) the OVOC emission ratio $\mathrm{ER_{OVOC}}$, (3) the hydrocarbon precursor emission ratio $\mathrm{ER_{HC}}$, and (4) the rate coefficient k_{HC} for the reaction between the hydrocarbon precursors

and OH. If the precursor hydrocarbon is known, its OH rate coefficient can be used for k_{HC}, but in general, no assumptions are made about the precursors, and k_{HC} represents the average rate coefficients of all precursors weighted by their abundance. The yield to form OVOC from the HC + OH reaction is taken as one, as the hydrocarbon emission ratio and yield cannot be independently determined from the fits. Similar equations were used before to analyze data sets from the Northeastern U.S. (de Gouw et al., 2005; Warneke et al., 2007) and from Beijing, China (Liu et al., 2009). In contrast with those analyses, we account for photolysis more explicitly in this work and omitted a biogenic source term from the analysis. Some of the OVOCs that are produced from hydrocarbon removal, such as glyoxal, do have important biogenic precursors (Washenfelder et al., 2011).

Examples of the results of fitting equation (6) to the data are shown in Figure 4 for three different OVOCs. The three terms in equation (6) determined from the fits are shown by the different colors. For each of the three OVOCs, the overall fit describes a significant fraction of the variability in the observations. These three compounds were chosen as examples of compounds with primarily photochemical sources (formic acid), direct emission sources (i-propanol), and both photochemical and emission sources (acetaldehyde). In case of formic acid, a background value of 880 ± 40 pptv is inferred from the fit of equation (6), which is much higher than measurements made offshore during CalNex (Crisp et al., 2014). The basic reason that the measured formic acid at night is attributed to a background is the lack of correlation with CO (Figure 2b). As described above, we hypothesize that a nighttime loss of formic acid by deposition may be responsible for this. This effect could lead to an overestimate of the background and an underestimate of the direct emission and photochemical formation contributions.

Analyses such as illustrated in Figure 4 are repeated for all measured oxygenates. Results of the fits are shown in Figure 5 as the average diurnal variations in the measurements and fit terms according to equation (6). The resulting emission ratios ER_{OVOC}, backgrounds, and the linear correlation coefficients between the data and fits are shown in Table 1. The fit values for ER_{HC} and k_{HC} are not shown: These parameters are strongly coupled in equation (6), and their fit values have large uncertainties. Formation of OVOCs from a smaller pool of more reactive precursors versus from a larger pool of less reactive precursors is hard to distinguish from the OVOC time series alone.

Uncertainties in the emission ratios ER_{OVOC} in Table 1 are determined from three different factors. First, random errors were determined from the fits. These were significant for those compounds that do not correlate well with CO, like the alcohols. Methanol most likely has high biogenic sources in the basin (Millet et al., 2008), and the higher alcohols are used as solvents in various chemical products (McDonald et al., 2018). Random errors also contributed for some organic acids, which were close to the detection limits of the acetate-ion chemical ionization mass spectrometry instrument. Second, the fits were repeated with the CO background at the low and high end of its uncertainty range (115 ± 10 ppbv) to quantify the associated error in the emission ratio. These errors tend to be the smallest for most compounds. Third, the fits were repeated with the uncertainty in the OH exposure at the low and high end of its uncertainty range (see companion paper for details; de Gouw et al., 2017). These errors tend to dominate for those compounds that have rapid photochemical formation such as the aldehydes and acids.

The effects of nighttime chemistry were considered in addition to those from OH chemistry during the day. The OVOC emission ratios ER_{OVOC} are strongly determined by the nighttime observations. Nighttime formation of OVOCs is not included in equation (6) and, if significant, could lead to overestimating the direct emissions in the analysis. It was shown in our companion paper that the removal of several reactive alkenes by ozone and NO_3 is significant at night (de Gouw et al., 2017), and this chemistry forms aldehydes and acids. Figure 6 shows the enhancement ratios versus CO of formic acid, i-propanol, and acetaldehyde as a function of the OH exposure in the left column, and as a function of nighttime ozone exposure in the right column. To calculate these enhancement ratios, backgrounds in both CO (115 ppbv) and the OVOCs (determined from fit of equation (6)) are subtracted from the measurements. The black curves in Figures 6a–6c show the fits of equation (6) to the data, with the open diamonds representing the emission ratios ER_{VOC} from the fits. The data for formic acid and acetaldehyde show a clear increase with OH exposure due to photochemical formation (Figures 6a and 6c). In contrast, the data for i-propanol show a slight decrease with OH exposure (Figure 6b), as this compound is not formed photochemically but is moderately reactive with OH (rate coefficient is 5.1×10^{-12} cm^3 $molecule^{-1}$ s^{-1}, Table 1). For formic acid, i-propanol, and acetaldehyde, the nighttime

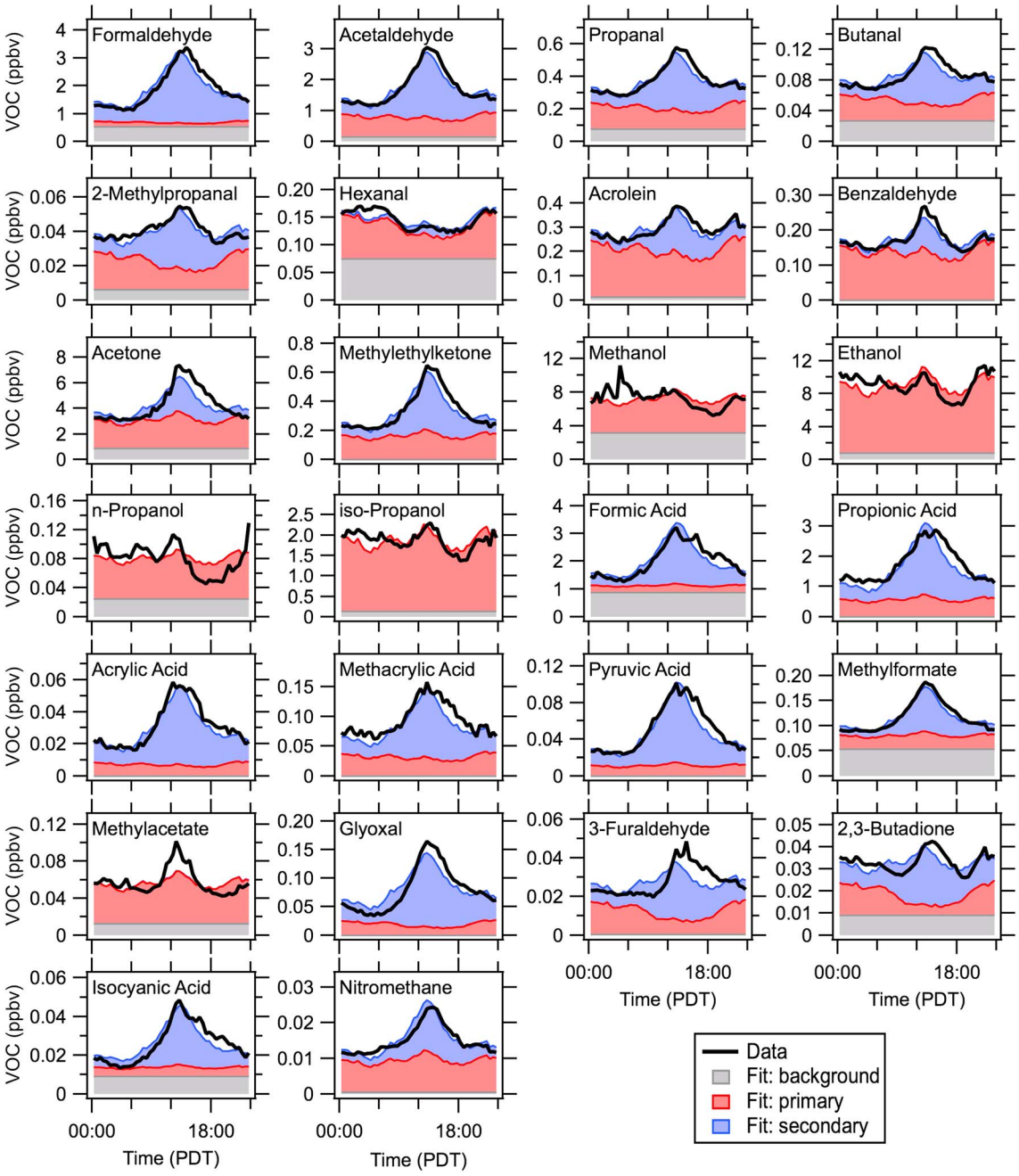

Figure 5. Diurnal variations of all oxygenated volatile organic compounds along with the results of the multivariate regression fits to the data.

data show only a weak dependence on ozone exposure (Figures 6d–6f). The same was found for all other OVOCs (Figure S5). The data are fit by a linear function of ozone exposure; the black curves in Figures 6d–6f show the results. There is a weak increase with nighttime ozone exposure for formic acid and acetaldehyde and a weak decrease for i-propanol. A linear function is used instead of a function similar to equation (6) that incorporates emission, formation, and removal as a function of ozone exposure; the dependence on ozone exposure was too weak to allow an analysis like that. The intercepts at zero ozone exposure can be interpreted as the OVOC emission ratios corrected for nighttime formation and are shown by the black diamonds in Figures 6d–6f. For the three OVOCs in Figure 6, these nighttime intercepts agree, or are slightly higher, than the values of ER_{OVOC} calculated from the entire data set using

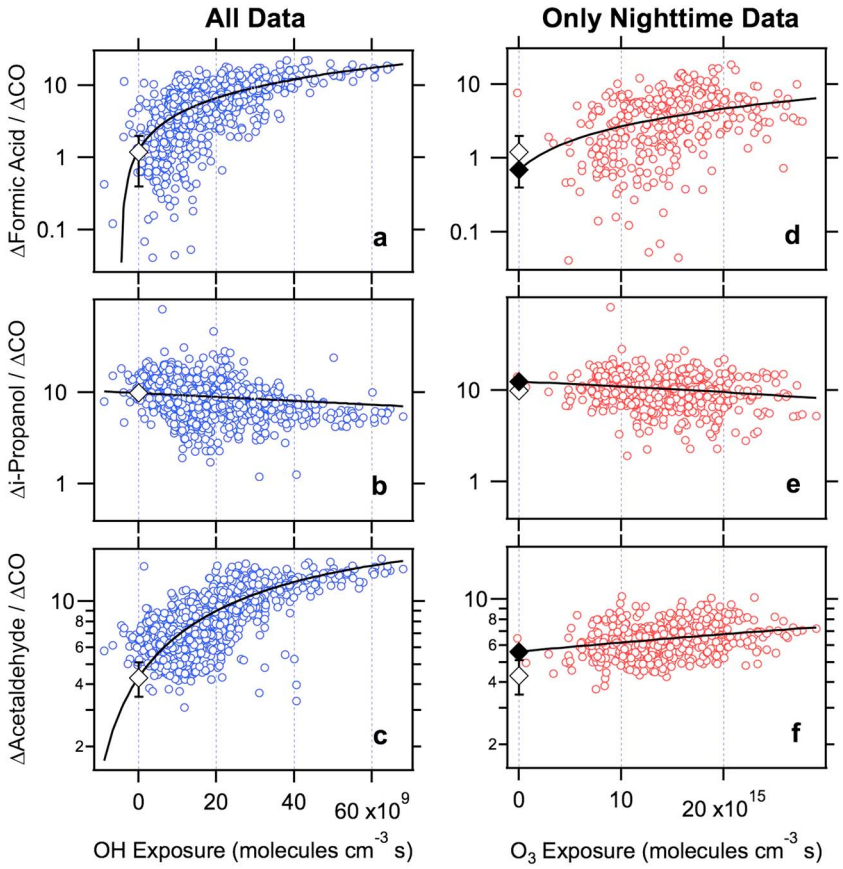

Figure 6. Ratios of three different oxygenated volatile organic compounds (formic acid, i-propanol, and acetaldehyde) versus CO (in units of pptv $[ppbv\ CO]^{-1}$) as a (left column) function of OH exposure (blue) and as a (right column) function of nighttime ozone exposure (red). The black curves in the left column represent fit results of equation (6) to the measurement data. The black lines in the right column show the results of linear fits to the data. The open diamonds and error bars in all panels represent the emission ratios derived from the fits of equation (6) incorporating all data. The solid black diamonds in the right column represent the emission ratios derived from the fits versus O_3 exposure incorporating nighttime data only.

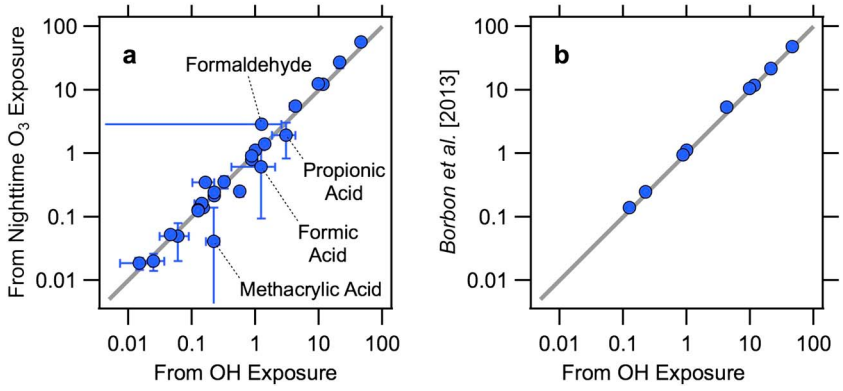

Figure 7. (a) Comparison between the oxygenated volatile organic compound (OVOC) emission ratios (in units of pptv $[ppbv\ CO]^{-1}$) determined from the fits of all data versus OH exposure using equation (6) and from the fits of nighttime data only versus ozone exposure. (b) Comparison of the presently reported OVOC emission ratios with results from our previous analysis of a subset of these compounds (Borbon et al., 2013).

equation (6) (shown again by the open diamonds in Figures 6d–6f). Figure 7a compares the emissions ratios for all OVOCs determined from the nighttime data only with those calculated from the whole data set using equation (6) and finds good agreement within the combined uncertainties. We conclude that there is only weak evidence for nighttime formation of OVOCs and that the process does not bias the calculated OVOC emission ratios in Table 1.

Figure 7b compares the OVOC emission ratios from this work (Table 1) with those from our previous analysis of a subset of these compounds (Borbon et al., 2013), which were determined from the nighttime OVOC versus CO ratios. The data value reported in Borbon et al. (2013) for benzaldehyde was incorrect due to a typo, and the correct value of 0.94 pptv $ppbv^{-1}$ is used in Figure 7b. Figure 7b shows good agreement between the two analyses: Emission ratios for OVOCs can accurately be determined from the correlation slopes of nighttime data only. This work extends the reported emission ratios in Borbon et al. (2013) to several more species derived from the GC-MS measurements (acrolein, 2-methylpropanal, hexanal, n-propanol, methylformate, methylacetate, 3-furaldehyde, and nitromethane) and to the measured formaldehyde, organic acids, and glyoxal data. The emission ratios will be discussed in some detail in section 3.4 below. In addition, this work allows the chemical formation of OVOCs to be quantified (Figure 5), and the results are discussed below in section 3.5.

3.3. Evaluation of Analysis Methods Using WRF-Chem Model

In the real atmosphere, OVOCs are released from a range of locations, and the emissions from these sources are chemically transformed and mixed with other air masses before reaching the sampling site. In contrast, the present analysis assumes that the composition of emissions is constant across the basin and uses a single value of OH exposure to describe the average degree of processing of the sampled emissions. The validity of these assumptions, and of the separation between emissions and chemistry resulting from our analysis, is further investigated here. In our companion paper, we addressed this issue using WRF-Chem model output for Pasadena (de Gouw et al., 2017). We analyzed the model output in the exact same way as the measurement data and showed that the hydrocarbon emission ratios calculated from the WRF-Chem model output agreed on average with the emissions inventory used as the WRF-Chem model input. We will extend that analysis here for three oxygenated species in the model: HCHO (formaldehyde), ALD (acetaldehyde and higher aldehydes), and KET (ketones) (Stockwell et al., 1997).

In the online supporting information, we show the following analyses in more detail:

1. Average diurnal variations of modeled OVOCs showed enhancements during the daytime relative to less reactive hydrocarbons (Figure S6). In contrast with the measurement data, the daytime enhancement in ALD species is not as pronounced compared to the measured acetaldehyde and higher aldehydes (Figure 5).
2. Scatterplots of modeled OVOCs versus modeled CO showed daytime enhancements of HCHO relative to CO, but the trends were weaker for ALD and KET compounds (Figure S6). Nighttime correlations with CO were not very strong ($0.392 < r^2 < 0.476$) and are notably weaker than observed in the measurement data (acetone: $r^2 = 0.711$; acetaldehyde: $r^2 = 0.858$; Figure S2). In our companion paper, we reported weaker correlations between the modeled hydrocarbons and CO than in the measurements and attributed this to differences in the diurnal variations of hydrocarbon and CO emissions used in WRF-Chem (de Gouw et al., 2017). The same is true for the OVOCs as shown in S8. CO emissions show a much larger enhancement during the daytime relative to the nighttime than the OVOCs do. As a result, the OVOC/CO emission ratios are much higher at night than during the daytime. What is also seen in Figure S8 is that the diurnal variations in the emissions of HCHO, ALD, and KET show different dependencies on the time of day, possibly caused by the relative importance of diesel versus gasoline emissions at different times of the day (Rappenglück et al., 2013).

The importance of daytime and nighttime formation of modeled OVOCs is studied in Figure 8. Model ratios between OVOCs and CO are shown as a function of OH exposure in the column on the left including all data, and as a function of ozone exposure in the column on the right using only nighttime data. The time series of HCHO, ALD, and KET are fit using equation (6), and the fit results are shown as a function of OH exposure in Figures 8a–8c. While the formaldehyde versus CO ratio increases with OH exposure, the ratios of ALD versus CO and of KET versus CO ratio do not depend very uniformly on OH exposure. However, in contrast with the

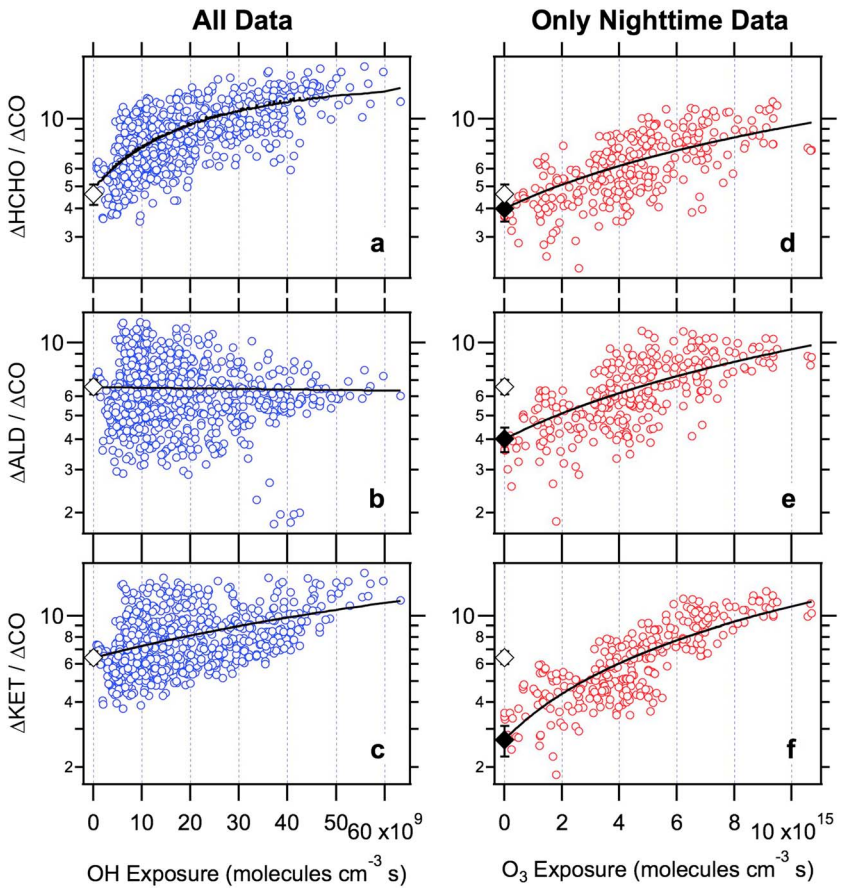

Figure 8. Ratios of three carbonyl compounds in the Weather Research and Forecasting-Chemistry model output for Pasadena versus CO (in pptv [ppbv CO]$^{-1}$) as a (left column) function of OH exposure (blue) and as a (right column) function of nighttime ozone exposure (red). The black curves in the left column represent fit results of equation (6) to the model data. The black curves in the right column show fit results of equation (7) to the model data. The open diamonds and error bars in all panels represent the emission ratios derived from the fits of equation (6) incorporating all model data. The solid black diamonds in the right column represent the emission ratios derived from the fits versus O_3 exposure incorporating nighttime model data only.

measurement data (Figure 6), the model output shows clear signs of nighttime formation of HCHO, ALD, and KET (Figures 8d–8f).

Part of the reason why nighttime formation of OVOCs is more efficient in the WRF-Chem model than observed in the measurements is due to the model treatment of olefins with internal bonds (OLI). Reactions of OLI with both ozone and NO_3 have high yields of OVOCs in the mechanism (Stockwell et al., 1997). We compared the emissions of OLI in the model with the emissions of all measured OLI species (Figure S9a) and found that the modeled emissions are a factor of 2.6 higher. Next, we compared the reaction rate coefficients for OLI with ozone and NO_3, respectively, with the average rate coefficients for the measured OLI species weighted by their emissions (Middleton et al., 1990). For the OLI + ozone reaction, we find that the model rate coefficient in RACM is a factor of 3.7 higher than the emission-weighted average rate coefficient for the measured OLI species (Figure S9b). We also considered an additional weighting factor in calculating the average that is derived from the reacted fraction of each OLI species at night. These so-called reactivity-weighting factors (Middleton et al., 1990) were calculated using a nighttime ozone exposure of 20×10^{15} molecules cm^{-3} s (Figure 6) and a compound-dependent enhancement in the removal rate by NO_3 (de Gouw et al., 2017). It was found that the reactivity-weighting factors were >0.86 for all OLI species (the nighttime removal was very efficient) and the reactivity-weighted average rate coefficients are therefore very similar to the emissions-weighted average rate coefficients. A similar conclusion was reported for calculating average

rate coefficients for the OLI + OH reactions in RACM (Middleton et al., 1990). For the OLI + NO_3 reaction, the model rate coefficient in RACM is 11 times higher than the emission-weighted average rate coefficient for the measured OLI species (Figure S9c). One of the most reactive hydrocarbons with ozone and NO_3 is 2-methyl-2-butene (Atkinson & Arey, 2003), which was not quantified from the measurements. This hydrocarbon can be incorporated into the analysis by assuming that it was emitted at the same rate relative to the measured alkenes as observed in motor vehicle exhaust (May et al., 2014). The RACM rate coefficients for the OLI + ozone and OLI + NO_3 reactions would still overestimate the emission-weighted average rate coefficients of OLI species by factors of 2.9 and 4.5, respectively. We conclude that nighttime formation of OVOCs in the model is more efficient than the measurements show because (1) 2011 National Emissions Inventory emissions of OLI are higher than found from the measurements and (2) because the RACM mechanism uses reaction rate coefficients for the OLI + ozone and OLI + NO_3 reactions that are significantly faster than the average rate coefficients of the measured OLI species weighted by their emissions. As a result, we find that a significant fraction of OVOCs in the model at night is secondary, whereas analysis of the measurements indicates that direct emissions are important for most aldehydes and ketones at night (Figure 5). Lowering the RACM rate coefficients for the OLI + ozone and OLI + NO_3 reactions should be considered in view of these findings and the detailed data on the emissions of OLI species available in the literature (May et al., 2014).

Figure 8 illustrates that OVOCs are formed in the model at night. This nighttime formation was not observed in the measurements, and emission ratios were determined from the measurements using fits of equation (6) to the data. Applying this same analysis to the model output would overestimate the emission ratios. To account for nighttime formation of the modeled OVOCs, equation (6) can be rewritten as

$$\mathrm{OVOC} = \mathrm{background} + \mathrm{ER_{OVOC}} \times \Delta\mathrm{CO} + \mathrm{ER_{HC}} \times \Delta\mathrm{CO} \times \left(1 - e^{-k_{\mathrm{HC+O3}}[\mathrm{O_3}]\Delta t}\right) \quad (7)$$

The simplification compared with equation (6) comes from the fact that CO, HCHO, ALD, and KET do not react with ozone in the RACM mechanism (and HCHO and ALD only very slowly with NO_3) (Stockwell et al., 1997). Equation (7) is fit to the modeled time series for HCHO, ALD, and KET (nighttime data only), using four free parameters: background, ER_{OVOC}, ER_{HC}, and k_{HC+O3}. The fit results are shown as a function of ozone exposure by the black curves in Figures 8d–8f. The emission ratios ER_{OVOC} are shown by the black diamonds in Figure 8, with the error bars representing the statistical error from the fits. The black diamonds intercept the black curves in Figures 8d–8f at zero ozone exposure, as the emission ratios have been calculated from these fits, but they are significantly lower than the OVOC emissions ratios calculated from the fits of equation (6) that only consider daytime chemistry (open diamonds in Figure 8). This is in contrast with the measurement data, which showed only weak evidence for nighttime formation (Figures 6d–6f) and for which the emission ratios calculated equation (6) agreed with the emission ratios calculated from the nighttime data (Figures 6d–6f and 7a).

To evaluate our method for calculating emission ratios, we can now compare the OVOC emission ratios calculated from the WRF-Chem model output with the ratios between OVOC and CO emissions used as WRF-Chem input. Figure 9 compares the emission ratios for HCHO, ALD, and KET and adds the same comparison for the lumped hydrocarbon species (see Table S2 for a description) that were presented in our companion paper (de Gouw et al., 2017). The OVOC emission ratios calculated from the model output do not agree as well with the inventory as for the hydrocarbons. While the calculated emission ratio of KET agrees closely with the inventory used in WRF-Chem, the calculated emission ratios of HCHO and ALD are both ~70% higher than in the inventory. This illustrates the difficulty in separating the effects of direct emissions and rapid chemical formation. It is likely that the issue is not as severe in the analysis of the measurements, since the measurement data showed only weak evidence for nighttime formation, and the nighttime data therefore provide better constraints on the emissions. Nevertheless, the analysis suggests that the calculation of direct OVOC emissions from surface measurements can be biased high by methods that account for photochemical aging, particularly for compounds that are rapidly formed in the atmosphere.

3.4. Comparison of OVOC Emissions With Other Studies

The OVOC emission ratios in Table 1 are analyzed in detail in a separate study that shows that many of the OVOCs have important sources from the use of volatile chemical products such as cleaners, glues,

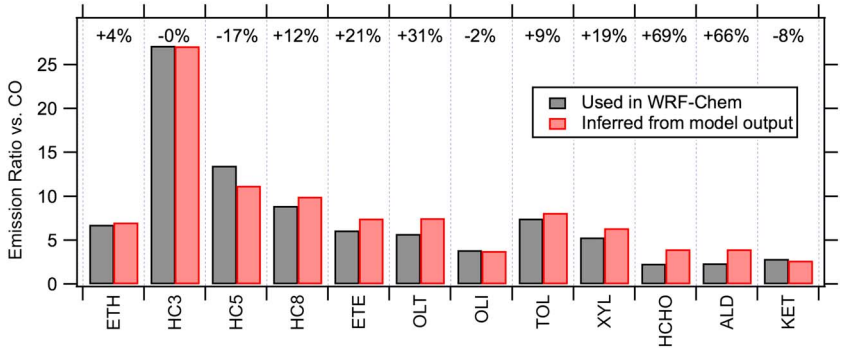

Figure 9. Comparison of emission ratios calculated from the Weather Research and Forecasting-Chemistry (WRF-Chem) model output for Pasadena versus those from the 2011 National Emissions Inventory inventory used in WRF-Chem (in pptv $[ppbv\ CO]^{-1}$). The percentage difference between the two results is shown near the top of the panel. See Table S2 for a description of the lumped species in Regional Atmospheric Chemistry Mechanism.

coatings, solvents, and personal care products (McDonald et al., 2018). Previous studies had noted that emission ratios of OVOCs are much higher than what can be explained from motor vehicle emissions (Borbon et al., 2013; Warneke et al., 2007). The new source attribution study explains many of these differences using a newly developed bottom-up inventory of emissions from the use of volatile chemical products (McDonald et al., 2018).

The aldehydes are one class of compounds that were not well explained by the new inventory of volatile chemical products (McDonald et al., 2018). As noted above, several of the aldehydes correlated strongly with CO at night when their chemical formation and removal was slow. This suggests that their emissions from motor vehicles are significant. Figure 10 compares the aldehyde emission ratios determined in this work with those from four tunnel (Ban-Weiss et al., 2008; Gentner et al., 2013; Kirchstetter, Singer, Harley, Kendall, & Hesson, 1999; Kirchstetter, Singer, Harley, Kendall, & Traverse, 1999; Legreid et al., 2007) and two dynamometer

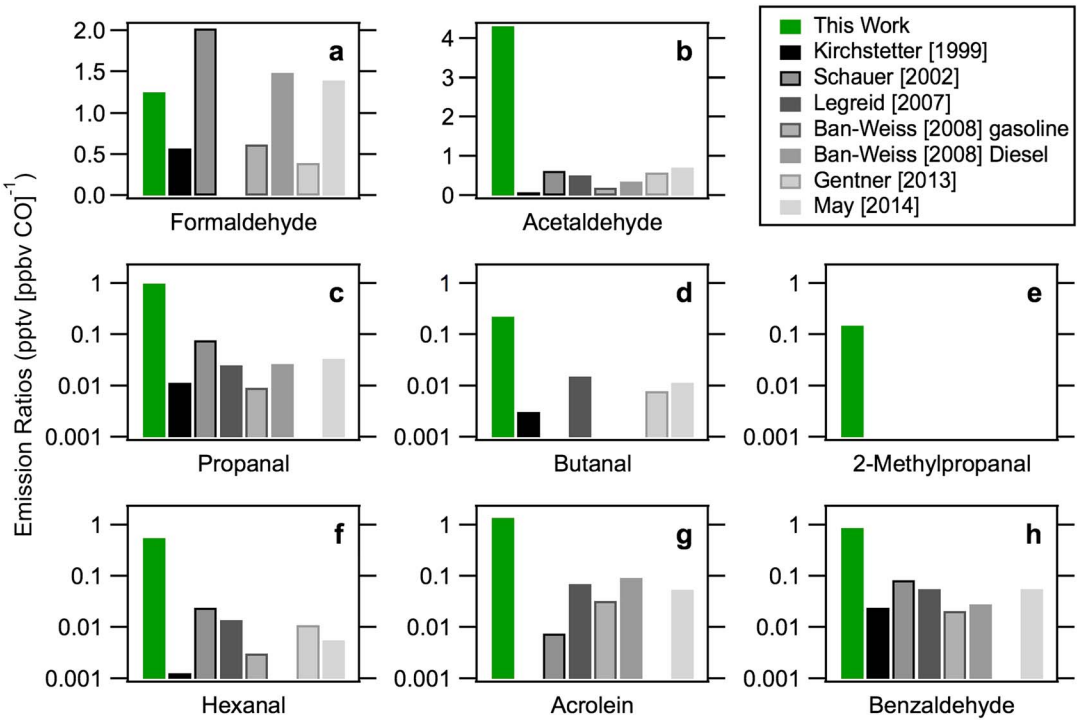

Figure 10. Comparison between oxygenated volatile organic compound emission ratios versus CO determined in this work and results from the literature.

studies of gasoline vehicles (May et al., 2014; Schauer et al., 2002). Except for formaldehyde, the emission ratios of aldehydes versus CO reported here are systematically higher than those found in tunnel and dynamometer studies (Figure 10).

Emission ratios for formaldehyde show some variability between studies, with our newly reported value in the range of previous results. Some of this variability is likely due to the relative importance of diesel versus gasoline vehicles in the different studies. Emissions from diesel engines are particularly rich in aldehydes (May et al., 2014; Schauer et al., 1999) but can be more difficult to determine separately from tunnel measurements. One tunnel study was used to separate gasoline and diesel emissions of carbonyls (Ban-Weiss et al., 2008). While the diesel emission ratios versus CO are higher than those from gasoline, both values are well below the emission ratios quantified in this study (Figure 10). Some other studies of formaldehyde versus CO emission ratios were not included in Figure 10a (Garcia et al., 2006). A value of 2.93 ± 0.13 pptv ppbv^{-1} was reported from roadside measurements in Houston, Texas (Rappenglück et al., 2013). An analysis of data from the Moody Tower in Houston arrived at a ratio of 3.0 ± 0.2 pptv ppbv^{-1} (Parrish et al., 2012). The latter study discussed the difficulties in obtaining these ratios from ambient measurements in detail.

The reasons for the discrepancies between ambient and motor-vehicle emission ratios for higher aldehydes (Figures 10b–10h) are unknown at present. A recent study showed that cold-start emissions of VOCs dominate over emissions from warmed-up vehicles for typical commuting distances of modern vehicles (Drozd et al., 2016), and cold starts are not captured by tunnel and dynamometer studies. However, CO emissions are also higher during cold starts, so VOC/CO ratios may not be affected as much. The same study argued that the contributions of highly emitting, that is, older and malfunctioning vehicles, on overall emissions are more important to consider than cold starts (Bishop et al., 2012). Tunnel and road side studies should capture emissions from highly emitting vehicles, but the statistics may be poor as a few individual vehicles can affect the average results of a study (Bishop et al., 2012). Other emission sources of aldehydes in urban air include those from cooking, which is a source of C6 and higher aldehydes (Gysel et al., 2017).

As shown in Figure 5, measurements of 3-furaldehyde were not well described by equation (6). Measurements of 3-furaldehyde on average rose sharply at noon and then lingered into the evening. It was one of the few OVOCs, for which a clear difference was observed between weekdays and weekends (Figure S10). Furaldehydes are known to be released from wood burning (Coggon et al., 2016; Gilman et al., 2015), and emissions from the Caltech cafeteria at approximately 400 m from the site, which was closed on weekends, are suspected to be the source of 3-furaldehyde.

3.5. Photochemical Formation of OVOCs

Photochemical formation of several OVOCs in this data set (formaldehyde, formic acid, glyoxal, and isocyanic acid) has been discussed previously in detail, and these compounds will not be further analyzed here (Chen et al., 2013; Roberts et al., 2014; Veres et al., 2011; Washenfelder et al., 2011; Yuan et al., 2015). Instead, we will focus on the photochemical formation of the newly reported species that have not been discussed elsewhere.

The measured time series of five species (2-methylpropanal, acrolein, benzaldehyde, methyl formate, and 2,3-butadione) were well described by equation (6), and photochemical formation was evident from the fits (Figure 5). For all five species, the number of known precursors is limited. In fitting equation (6) to the measured time series, we previously treated both the emission ratio of the precursors (ER_{HC}) and their reaction rate coefficients with OH (k_{HC}) as free variables. As these parameters are strongly coupled in equation (6), the resulting fit parameters have large uncertainties. However, if we know the precursor, we can fix k_{HC} at the rate coefficient for that compound and get a more precise estimate of the emission ratio ER_{HC} that is consistent with the data. This analysis was performed for 2-methylpropanal, acrolein, benzaldehyde, methyl formate, and 2,3-butadione, and the results are shown in Table 2. For each of these OVOCs, the known precursors are listed in the second column, their reaction rate coefficients with OH in the third column, and their emission ratios versus CO from previous work are in the fourth column. For 3-methyl-1-butene, 1,3-butadiene, styrene, o-xylene, 1,2,3-trimethylbenzene, and 1,2,4-trimethylbenzene, these emission ratios were determined from our own measurements and reported in the companion paper (de Gouw et al., 2017). Dimethyl ether was not measured in this work, but the compound is included in the inventory of volatile chemical product emissions (McDonald et al., 2018). The molar yields for the precursor to form the OVOC

Table 2
Comparison of the Precursor Emission Ratios Needed to Explain the Formation of Four Specific Oxygenated Volatile Organic Compounds With Values for Expected Precursors From the Literature

Product	Precursor	k_{HC}[a] cm^3 $molec^{-1}$ s^{-1}	ER From lit.	Yield[b] From Master Chemical Mechanism	ER_{HC} Expected	ER_{HC} From fit
2-Methylpropanal	3-Methyl-1-butene	3.18×10^{-11}	0.068[c]	94%	0.064	0.36
Acrolein	1,3-Butadiene	6.66×10^{-11}	0.40[c]	73%	0.29	0.96
Benzaldehyde	Styrene	5.8×10^{-11}	0.36[c]	100%	0.36	0.44
Methylformate	Dimethyl ether	2.8×10^{-12}	1.7[d]	99%	1.7	4.2
2,3-Butadione	o-Xylene	1.36×10^{-11}	0.77[c]	17%	0.31	0.45[e]
	1,2,3-Trimethylbenzene	3.27×10^{-11}	0.29[c]	38%		
	1,2,4-Trimethylbenzene	3.25×10^{-11}	0.79[c]	8.6%		

Note. See text for more details. All emission ratios in units of pptv $[ppbv\ CO]^{-1}$.
[a]Atkinson and Arey (2003). [b]Saunders et al. (2003). [c]de Gouw et al. (2017). [d]McDonald et al. (2018). [e]Rate coefficient k_{HC} used in the fit is the weighted average for the three precursors (24.6×10^{-12} cm^3 $molecule^{-1}$ s^{-1}).

in the MCM are shown in the fifth column, where it is assumed that nitrogen oxide concentrations were high enough to favor RO_2 + NO over RO_2 + HO_2 reactions. The expected values of ER_{HC} in equation (6) are calculated as the precursor emission ratios (fourth column) multiplied by the yields (fifth column). These expected values of ER_{HC} can finally be compared with the values of ER_{HC} derived from the fits of the OVOC time series.

For benzaldehyde, 82% of the formation can be explained from the removal of styrene. For 2,3-butadione, 69% of the formation can be explained from the removal of three aromatic hydrocarbons with two methyl groups in ortho positions. In the other cases, the expected values of ER_{HC} are smaller (by up to a factor of 6) than the values obtained from the fit, suggesting, perhaps not surprisingly, that other precursors play a role.

For methylformate, 40% of the formation can be explained from the removal of dimethyl ether. In this case, it should be noted that the emission ratio of dimethyl ether was not determined from this data set but taken from the emission inventory of volatile chemical product emissions (McDonald et al., 2018). Dimethyl ether is a highly volatile compound that is used as a propellant in products such as hairspray and bug spray. A difference of a factor of 2.5 between modeled and actual emissions is just outside the differences seen for most other compounds between the measurements and the volatile chemical product emissions inventory (McDonald et al., 2018).

In contrast with methylformate, the fit of equation (6) to the methylacetate data did not show a significant secondary source (Figure 5). The measurement data did show an average enhancement around noon that is poorly resolved by the fit of equation (6). By analogy with the formation of methylformate ($CH_3OC(O)H$) from dimethyl ether (CH_3OCH_3), methylacetate ($CH_3OC(O)CH_3$) could be formed from methyl ethyl ether ($CH_3OC_2H_5$), but this compound is not included in the MCM. For diethyl ether, which is included in the MCM, the abstraction of a hydrogen atom results in the formation of ethylformate ($C_2H_5OC(O)H$). By analogy, it is more likely that methyl ethyl ether will form ethylformate and/or methylformate. Also, methyl ethyl ether is not present in the inventory of volatile chemical product emissions (McDonald et al., 2018) and its emissions may be smaller than those of dimethyl ether. These arguments make it plausible why formation of methylacetate was not observed.

The data for nitromethane were described well by equation (6), and photochemical formation was inferred from the fit (Figure 5). Nitromethane is used as a solvent and as an engine fuel in motor sports and hobby aircraft. It is also present in diesel exhaust (Sekimoto et al., 2013). However, there are no known reaction pathways to form nitromethane in the atmosphere. Nitromethane can be formed from association reactions between methyl radicals and NO_2 (Glaenzer & Troe, 1974), but in the atmosphere, this reaction cannot compete with the formation of methylperoxy (CH_3O_2) radicals and their subsequent reactions with NO and HO_2. Enhanced emissions of nitromethane during the day or measurement issues might be alternative explanations for its daytime enhancement (Figure 5).

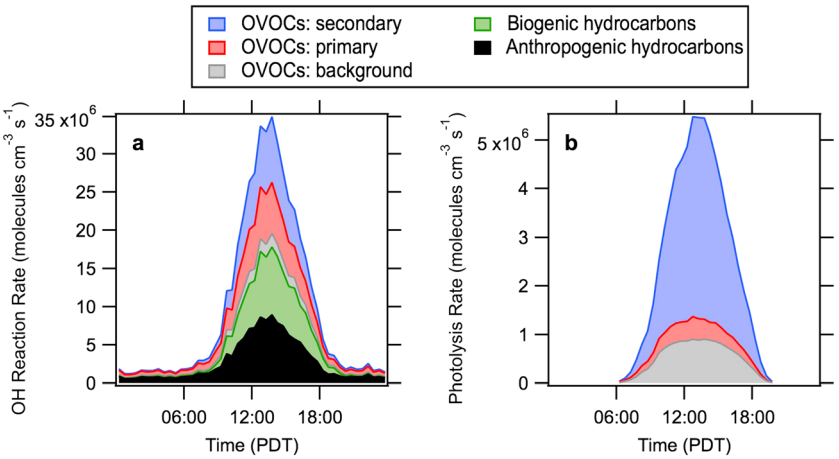

Figure 11. (a) Reaction rate of measured hydrocarbons and oxygenated volatile organic compounds (OVOCs) with OH. (b) Photolysis rates of measured OVOCs. The contributions of OVOCs from direct emissions (primary), chemical formation (secondary), and backgrounds are separated using the results from this work.

3.6. Implications for Ozone Formation

Oxygenated VOCs contribute in two important ways to urban photochemistry. OVOCs represent a significant fraction of the reactivity with OH, and some OVOCs can be photolyzed and be a source of radicals. Both processes are quantified here with the contributions from OVOCs from primary and secondary sources separated according to our previous analysis (Figure 5).

Figure 11a shows the calculated, average diurnal variation in the total OH reaction rates of the anthropogenic hydrocarbons (reported in our companion paper) (de Gouw et al., 2017), biogenic hydrocarbons, and OVOCs. The OVOCs have been split into contributions from background, direct emissions, and chemical formation using the results shown in Figure 5. The contribution from directly emitted OVOCs to OH reaction rates was significant at all times of the day, and OVOCs clearly need to be accurately represented in emissions models to describe ozone chemistry. One important contributor to the OH reaction rates were alcohols released from volatile chemical products (McDonald et al., 2018) and the use of gasoline blended with ethanol (de Gouw et al., 2012). Alcohols are not particularly reactive with OH, but they did have large emissions during CalNex (Table 1). The second important contributor to the OH reaction rates were aldehydes from sources that are still poorly understood as described in section 3.4. The large contribution during the day from biogenic VOCs, particularly isoprene, to the OH reaction rates is also notable (Figure 11a). Pasadena is more densely vegetated than areas upwind of it, so the isoprene measurements at this site may not be fully representative for the entire footprint of the measurements. Nevertheless, analysis of the glyoxal data has shown that isoprene is a significant precursor (Washenfelder et al., 2011), and the same is likely true for formaldehyde.

Figure 11b shows the average diurnal variation in total photolysis rates of OVOCs with the contributions from secondary and primary sources, and the background separately indicated. The total OVOC photolysis is strongly determined by formaldehyde and secondary sources dominate. Separate analyses have shown that OVOC photolysis represents 29–40% of the total radical production at the surface, with the rest coming from the $O(^1D) + H_2O$ reaction, $ClNO_2$ and HONO photolysis, and ozone + alkene reactions (Griffith et al., 2016; Young et al., 2012).

4. Conclusions

In this work, we analyzed an extensive data set of OVOCs obtained by several instruments in the Los Angeles basin during the NOAA CalNex study in 2010. The number of OVOCs determined from the GC-MS measurements was expanded using new peak-fitting software. Using the data for CO as an emissions tracer and the OH exposure calculated from hydrocarbon ratios, we separated the effects of direct OVOC emissions from their chemical formation and removal. Evidence for nighttime formation of OVOCs was only weak.

The analysis method is evaluated using output from the chemistry-transport model WRF-Chem for Pasadena. The model output is analyzed in the same manner as the measurement data. The WRF-Chem model shows significant nighttime formation of aldehydes and ketones, which is not supported by evidence from the measurements. Nighttime formation of OVOCs is stronger in the model because precursor emissions are higher than the measurements indicate, and the reaction rate coefficients for the precursors with ozone and NO_3 are faster in the reaction mechanism than for the measured precursor hydrocarbons. To determine OVOC emissions from the model output, the nighttime chemical formation of OVOCs is accounted for by using the ozone exposure calculated from hydrocarbon ratios. The OVOC emission ratios versus CO, determined from the WRF-Chem model output after accounting for nighttime formation, overestimate the OVOC emission ratios in the inventory by up to ~70%. This analysis provides some constraints on how accurately OVOC emission ratios can be determined from the measurements, although the error is likely smaller in the measurement data that show stronger OVOC versus CO correlations and only weak evidence for nighttime formation of OVOCs. The error is also likely to be small for OVOCs that do not have secondary sources such as the alcohols.

The correlation between most measured aldehydes and CO at night suggests a contribution from motor vehicle emissions. However, the emission ratios of most aldehydes versus CO are higher than those from motor vehicle emissions, so the aldehyde sources in urban air remain unclear.

Formation of several OVOCs is investigated in terms of the removal of specific precursors. For example, it is found that 82% of the formation of benzaldehyde can be attributed to removal of styrene. Formation of methylformate constrains the emissions of its precursor dimethyl ether, which is used as a propellant in products such as hairspray and bug spray but was not quantified in this study. The emission ratio of dimethyl ether versus CO needed to explain the methylformate formation agrees within a factor of 2.5 of an emission estimate, suggesting that it is potentially formed from anthropogenic precursor emissions.

Finally, the direct emissions of OVOCs, notably alcohols and aldehydes, contribute significantly to OH reactivity throughout the day, and their emissions should be accurately represented in models to describe and predict ozone pollution.

Acknowledgments

Data used in this study can be found at http://www.esrl.noaa.gov/csd/projects/calnex/. We gratefully acknowledge support from the California Institute of Technology and Prof. John Seinfeld for hosting the ground site during CalNex. Funding from the California Air Resources Board for the site infrastructure is greatly appreciated. Si-Wan Kim acknowledges support from the NASA ROSES ACMAP program (NNH14AX01I). The OH measurements were supported by grants from the National Science Foundation (AGS-0612738 and AGS-1104880). The LP-DOAS measurements of formaldehyde were supported by a grant from the California Air Resources Board (ARB 08-318). The CE-DOAS measurements of glyoxal were supported by the National Science Foundation CAREER award ATM-847793. One of us (JdG) was associated with Aerodyne Research Inc. as a consultant during part of the preparation phase of the manuscript.

References

Ahmadov, R., McKeen, S., Trainer, M., Banta, R., Brewer, A., Brown, S., et al. (2015). Understanding high wintertime ozone pollution events in an oil and natural gas-producing region of the western US. *Atmospheric Chemistry and Physics*, *15*(1), 411–429. https://doi.org/10.5194/acpd-14-20295-2014

Al Mulla, I., Viera, L., Morris, R., Sidebottom, H., Treacy, J., & Mellouki, A. (2010). Kinetics and mechanisms for the reactions of ozone with unsaturated oxygenated compounds. *Chemphyschem*, *11*, 4069–4078.

Atkinson, R. (1986). Kinetics and mechanisms of the gas-phase reactions of the hydroxyl radical with organic compounds under atmospheric conditions. *Chemical Reviews*, *86*(1), 69–201. https://doi.org/10.1021/cr00071a004

Atkinson, R. (1991). Kinetics and mechanisms of the gas-phase reactions of the NO3 radical with organic compounds. *Journal of Physical and Chemical Reference Data*, *20*(3), 459–507. https://doi.org/10.1063/1.555887

Atkinson, R., & Arey, J. (2003). Atmospheric degradation of volatile organic compounds. *Chemical Reviews*, *103*(12), 4605–4638. https://doi.org/10.1021/cr0206420

Atkinson, R., Baulch, D. L., Cox, R. A., Hampson, R. F. Jr. Kerr, J. A., Rossi, M. J., & Troe, J. (1997). Evaluated kinetic, photochemical and heterogeneous data for atmospheric chemistry: Supplement V. *Journal of Physical and Chemical Reference Data*, *26*(3), 521–1011. https://doi.org/10.1063/1.556011

Ban-Weiss, G., Mclaughlin, J., Harley, R. A., Kean, A., Grosjean, E., & Grosjean, D. (2008). Carbonyl and nitrogen dioxide emissions from gasoline- and diesel-powered motor vehicles. *Environmental Science & Technology*, *42*(11), 3944–3950.

Bernard, F., Magneron, I., Eyglunent, G., Daële, V., Wallington, T. J., Hurley, M. D., & Mellouki, A. (2013). Atmospheric chemistry of benzyl alcohol: Kinetics and mechanism of reaction with OH radicals. *Environmental Science & Technology*, *47*(7), 3182–3189. https://doi.org/10.1021/es304600z

Bierbach, A., Barnes, I., & Becker, K. H. (1995). Product and kinetic study of the OH-initiated gas-phase oxidation of furan, 2-methylfuran and furanaldehydes at 300 K. *Atmospheric Environment*, *29*(19), 2651–2660. https://doi.org/10.1016/1352-2310(95)00096-H

Bishop, G. A., Schuchmann, B. G., Stedman, D. H., & Lawson, D. R. (2012). Multispecies remote sensing measurements of vehicle emissions on Sherman Way in Van Nuys, California. *Journal of the Air & Waste Management Association*, *62*(10), 1127–1133. https://doi.org/10.1080/10962247.2012.699015

Bon, D. M., Ulbrich, I. M., de Gouw, J. A., Warneke, C., Kuster, W. C., Alexander, M. L., et al. (2011). Measurements of volatile organic compounds at a suburban ground site (T1) in Mexico City during the MILAGRO 2006 campaign: Measurement comparison, emission ratios, and source attribution. *Atmospheric Chemistry and Physics*, *11*(6), 2399–2421. https://doi.org/10.5194/acp-11-2399-2011

Borbon, A., Gilman, J. B., Kuster, W. C., Grand, N., Chevaillier, S., Colomb, A., et al. (2013). Emission ratios of anthropogenic volatile organic compounds in northern mid-latitude megacities: Observations versus emission inventories in Los Angeles and Paris. *Journal of Geophysical Research; Atmospheres*, *118*, 2041–2057. https://doi.org/10.1002/jgrd.50059

Brophy, P., & Farmer, D. K. (2015). A switchable reagent ion high resolution time-of-flight chemical ionization mass spectrometer for real-time measurement of gas phase oxidized species: Characterization from the 2013 southern oxidant and aerosol study. *Atmospheric Measurement Techniques*, *8*(7), 2945–2959. https://doi.org/10.5194/amt-8-2945-2015

Cai, C., Geng, F., Tie, X., Yu, Q., & An, J. (2010). Characteristics and source apportionment of VOCs measured in Shanghai, China. *Atmospheric Environment*, *44*(38), 5005–5014. https://doi.org/10.1016/j.atmosenv.2010.07.059

Carter, W. P. L. (1994). Development of ozone reactivity scales for volatile organic compounds. *Journal of the Air & Waste Management Association*, *44*(7), 881–899. https://doi.org/10.1080/1073161X.1994.10467290

Chen, D., Li, Q., Stutz, J., Mao, Y., Zhang, L., Pikelnaya, O., et al. (2013). WRF-Chem simulation of NOx and O3 in the L.A. basin during CalNex-2010. *Atmospheric Environment*, *81*, 421–432. https://doi.org/10.1016/j.atmosenv.2013.08.064

Coggon, M. M., Veres, P. R., Yuan, B., Koss, A., Warneke, C., Gilman, J. B., et al. (2016). Emissions of nitrogen-containing organic compounds from the burning of herbaceous and arboraceous biomass: Fuel composition dependence and the variability of commonly used nitrile tracers. *Geophysical Research Letters*, *43*, 9903–9912. https://doi.org/10.1002/2016GL070562

Colmenar, I., Cabanas, B., Martinez, E., Salgado, M. S., & Martin, P. (2012). Atmospheric fate of a series of furanaldehydes by their NO3 reactions. *Atmospheric Environment*, *54*, 177–184. https://doi.org/10.1016/j.atmosenv.2012.02.087

Crisp, T. A., Brady, J. M., Cappa, C. D., Collier, S., Forestieri, S. D., Kleeman, M. J., et al. (2014). On the primary emission of formic acid from light duty gasoline vehicles and ocean-going vessels. *Atmospheric Environment*, *98*, 426–433. https://doi.org/10.1016/j.atmosenv.2014.08.070

Dagaut, P., Wallington, T. J., Liu, R., & Kurylo, M. J. (1988). A kinetics investigation of the gas-phase reactions of OH radicals with cyclic ketones and diones: Mechanistic insights. *The Journal of Physical Chemistry*, *92*(15), 4375–4377. https://doi.org/10.1021/j100326a026

de Gouw, J. A., Gilman, J. B., Borbon, A., Warneke, C., Kuster, W. C., Goldan, P. D., et al. (2012). Increasing atmospheric burden of ethanol in the United States. *Geophysical Research Letters*, *39*, L15803. https://doi.org/10.1029/2012GL052109

de Gouw, J. A., Gilman, J. B., Kim, S. W., Lerner, B. M., Isaacman-VanWertz, G., McDonald, B. C., et al. (2017). Chemistry of volatile organic compounds in the Los Angeles Basin: Nighttime removal of alkenes and determination of emission ratios. *Journal of Geophysical Research: Atmospheres*, *122*, 11,843–11,861. https://doi.org/10.1002/2017JD027459

de Gouw, J. A., Middlebrook, A. M., Warneke, C., Goldan, P. D., Kuster, W. C., Roberts, J. M., et al. (2005). Budget of organic carbon in a polluted atmosphere: Results from the New England Air Quality Study in 2002. *Journal of Geophysical Research*, *110*, D16305. https://doi.org/10.1029/2004JD005623

Derwent, R. G., Jenkin, M. E., & Saunders, S. M. (1996). Photochemical ozone creation potentials for a large number of reactive hydrocarbons under European conditions. *Atmospheric Environment*, *30*(2), 181–199. https://doi.org/10.1016/1352-2310(95)00303-G

Drozd, G. T., Zhao, Y., Saliba, G., Frodin, B., Maddox, C., Weber, R. J., et al. (2016). Time resolved measurements of speciated tailpipe emissions from motor vehicles: Trends with emission control technology, cold start effects, and speciation. *Environmental Science & Technology*, *50*(24), 13,592–13,599. https://doi.org/10.1021/acs.est.6b04513

El Boudali, A., Le Calve, S., Le Bras, G., & Mellouki, A. (1996). Kinetic studies of OH reactions with a series of acetates. *The Journal of Physical Chemistry*, *100*, 12,364–12,368.

Garcia, A. R., Volkamer, R., Molina, L. T., Molina, M. J., Samuelson, J., Mellqvist, J., et al. (2006). Separation of emitted and photochemical formaldehyde in Mexico City using a statistical analysis and a new pair of gas-phase tracers. *Atmospheric Chemistry and Physics*, *6*(12), 4545–4557. https://doi.org/10.5194/acp-6-4545-2006

Gentner, D. R., Worton, D. R., Isaacman, G., Davis, L. C., Dallmann, T. R., Wood, E. C., et al. (2013). Chemical composition of gas-phase organic carbon emissions from motor vehicles and implications for ozone production. *Environmental Science & Technology*, *47*(20), 11,837–11,848. https://doi.org/10.1021/es401470e

Gerbig, C., Smitgen, S., Kley, D., Volz-Thomas, A., Dewey, H., & Haaks, D. (1999). An improved fast response vacuum UV resonance fluorescence CO instrument. *Journal of Geophysical Research*, *104*, 1699–1704. https://doi.org/10.1029/1998JD100031

Gilman, J. B., Burkhart, J. F., Lerner, B. M., Williams, E. J., Kuster, W. C., Goldan, P. D., et al. (2010). Ozone variability and halogen oxidation within the Arctic and sub-Arctic springtime boundary layer. *Atmospheric Chemistry and Physics*, *10*(21), 10,223–10,236. https://doi.org/10.5194/acp-10-10223-2010

Gilman, J. B., Lerner, B. M., Kuster, W. C., Goldan, P. D., Warneke, C., Veres, P. R., et al. (2015). Biomass burning emissions and potential air quality impacts of volatile organic compounds and other trace gases from temperate fuels common in the United States. *Atmospheric Chemistry and Physics*, *15*(24), 13,915–13,938. https://doi.org/10.5194/acp-15-13915-2015

Glaenzer, K., & Troe, J. (1974). Reactions of alkyl radicals in the shock wave-induced pyrolysis of nitroalkanes. *Berichte der Bunsengesellschaft für Physikalische Chemie*, *78*, 182–184.

Goldan, P. D., Kuster, W. C., Williams, E. J., Murphy, P. C., Fehsenfeld, F. C., & Meagher, J. F. (2004). Nonmethane hydrocarbon and oxy hydrocarbon measurements during the 2002 New England Air Quality Study. *Journal of Geophysical Research*, *109*, D21309. https://doi.org/10.1029/2003JD004455

Grell, G. A., Peckham, S. E., Schmitz, R., McKeen, S. A., Frost, G., Skamarock, W. C., & Eder, B. (2005). Fully coupled "online" chemistry within the WRF model. *Atmospheric Environment*, *39*(37), 6957–6975. https://doi.org/10.1016/j.atmosenv.2005.04.027

Griffith, S. M., Hansen, R. F., Dusanter, S., Michoud, V., Gilman, J. B., Kuster, W. C., et al. (2016). Measurements of hydroxyl and hydroperoxy radicals during CalNex-LA: Model comparisons and radical budgets. *Journal of Geophysical Research: Atmospheres*, *121*, 4211–4232. https://doi.org/10.1002/2015JD024358

Guo, H., Wang, T., & Louie, P. K. K. (2004). Source apportionment of ambient non-methane hydrocarbons in Hong Kong. *Environmental Pollution*, *129*(3), 489–498. https://doi.org/10.1016/j.envpol.2003.11.006

Gysel, N., Welch, W. A., Chen, C.-L., Dixit, P., Cocker, D. R. III, & Karavalakis, G. (2017). Particulate matter emissions and gaseous air toxic pollutants from commercial meat cooking operations. *Journal of Environmental Sciences*, 1–9. https://doi.org/10.1016/j.jes.2017.03.022

Hak, C., Pundt, I., Trick, S., Kern, C., Platt, U., Dommen, J., et al. (2005). Intercomparison of four different in-situ techniques for ambient formaldehyde measurements in urban air. *Atmospheric Chemistry and Physics*, *5*(11), 2881–2900. https://doi.org/10.5194/acp-5-2881-2005

Isaacman-VanWertz, G., Sueper, D., Aikin, K. C., Lerner, B. M., Gilman, J. B., de Gouw, J. A., et al. (2017). Automated single-ion peak fitting as an efficient approach for analyzing complex chromatographic data. *Journal of Chromatography. A*, *1529*, 81–92. https://doi.org/10.1016/j.chroma.2017.11.005

Jorquera, H., & Rappenglück, B. (2004). Receptor modeling of ambient VOC at Santiago, Chile. *Atmospheric Environment*, *38*(25), 4243–4263. https://doi.org/10.1016/j.atmosenv.2004.04.030

Kim, S.-W., Heckel, A., Frost, G. J., Richter, A., Gleason, J., Burrows, J. P., et al. (2009). NO2 columns in the western United States observed from space and simulated by a regional chemistry model and their implications for NOx emissions. *Journal of Geophysical Research*, *114*, D11301. https://doi.org/10.1029/2008JD011343

Kim, S.-W., McDonald, B. C., Baidar, S., Brown, S. S., Dube, B., Ferrare, R. A., et al. (2016). Modeling the weekly cycle of NOx and CO emissions and their impacts on O3 in the Los Angeles-South Coast Air Basin during the CalNex 2010 field campaign. *Journal of Geophysical Research: Atmospheres*, *121*, 1340–1360. https://doi.org/10.1002/2015JD024292

Kirchstetter, T. W., Singer, B. C., Harley, R. A., Kendall, G. R., & Hesson, J. M. (1999). Impact of California reformulated gasoline on motor vehicle emissions. 2. Volatile organic compound speciation and reactivity. *Environmental Science & Technology*, *33*(2), 329–336. https://doi.org/10.1021/es980374g

Kirchstetter, T. W., Singer, B. C., Harley, R. A., Kendall, G. R., & Traverse, M. (1999). Impact of California reformulated gasoline on motor vehicle emissions. 1. Mass emission rates. *Environmental Science & Technology*, *33*(2), 318–328. https://doi.org/10.1021/es9803714

Lee, Y. N., Zhou, X., Kleinman, L. I., Nunnermacker, L. J., Springston, S. R., Daum, P. H., et al. (1998). Atmospheric chemistry and distribution of formaldehyde and several multioxygenated carbonyl compounds during the 1995 Nashville/Middle Tennessee Ozone Study. *Journal of Geophysical Research*, *103*, 22,449–22,462. https://doi.org/10.1029/98JD01251

Legreid, G., Balzani Loov, J., Staehelin, J. A. S., Hueglin, C., Hill, M., Buchmann, B., et al. (2007). Oxygenated volatile organic compounds (OVOCs) at an urban background site in Zurich (Europe): Seasonal variation and source allocation. *Atmospheric Environment*, *41*(38), 8409–8423. https://doi.org/10.1016/j.atmosenv.2007.07.026

Legreid, G., Reimann, S., Steinbacher, M., Staehelin, J. A. S., Young, D., & Stemmler, K. (2007). Measurements of OVOCs and NMHCs in a Swiss highway tunnel for estimation of road transport emissions. *Environmental Science & Technology*, *41*(20), 7060–7066. https://doi.org/10.1021/es062309

Leuchner, M., & Rappenglück, B. (2010). VOC source-receptor relationships in Houston during TexAQS-II. *Atmospheric Environment*, *44*(33), 4056–4067. https://doi.org/10.1016/j.atmosenv.2009.02.029

Liu, R., Huie, R. E., & Kurylo, M. J. (1990). The gas phase reactions of hydroxyl radicals with a series of nitroalkanes over the temperature range 240–400K. *Chemical Physics Letters*, *167*(6), 519–523. https://doi.org/10.1016/0009-2614(90)85462-L

Liu, Y., Shao, M., Kuster, W. C., Goldan, P. D., Li, X., Lu, S., & de Gouw, J. A. (2009). Source identification of reactive hydrocarbons and oxygenated VOCs in the summertime in Beijing. *Environmental Science & Technology*, *43*(1), 75–81. https://doi.org/10.1021/es801716n

May, A. A., Nguyen, N. T., Presto, A. A., Gordon, T. D., Lipsky, E. M., Karve, M., et al. (2014). Gas- and particle-phase primary emissions from in-use, on-road gasoline and diesel vehicles. *Atmospheric Environment*, *88*, 247–260. https://doi.org/10.1016/j.atmosenv.2014.01.046

McDonald, B. C., Dallmann, T. R., Martin, E. W., & Harley, R. A. (2012). Long-term trends in nitrogen oxide emissions from motor vehicles at national, state, and air basin scales. *Journal of Geophysical Research*, *117*, D00V18. https://doi.org/10.1029/2012JD018304

McDonald, B. C., Gentner, D. R., Goldstein, A. H., & Harley, R. A. (2013). Long-term trends in motor vehicle emissions in U.S. urban areas. *Environmental Science & Technology*, *47*(17), 10,022–10,031. https://doi.org/10.1021/es401034z

McDonald, B. C., McBride, Z. C., Martin, E. W., & Harley, R. A. (2014). High-resolution mapping of motor vehicle carbon dioxide emissions. *Journal of Geophysical Research: Atmospheres*, *119*, 5283–5298. https://doi.org/10.1002/2013JD021219

McDonald, B. C., de Gouw, J. A., Gilman, J. B., Jathar, S. H., Akherati, A., Cappa, C. D., et al. (2018). Volatile chemical products emerging as largest petrochemical source of urban organic emissions. *Science*, *359*(6377), 760–764. https://doi.org/10.1126/science.aaq0524

Mellouki, A., & Mu, Y. (2003). On the atmospheric degradation of pyruvic acid in the gas phase. *Journal of Photochemistry and Photobiology A: Chemistry*, *157*(2-3), 295–300. https://doi.org/10.1016/S1010-6030(03)00070-4

Middleton, P., Stockwell, W. R., & Carter, W. P. L. (1990). Aggregation and analysis of volatile organic compound emissions for regional modeling. *Atmospheric Environment*, *24A*, 1107–1133.

Millet, D. B., Jacob, D. J., Custer, T. G., de Gouw, J. A., Goldstein, A. H., Karl, T., et al. (2008). New constraints on terrestrial and oceanic sources of atmospheric methanol. *Atmospheric Chemistry and Physics*, *8*(23), 6887–6905. https://doi.org/10.5194/acp-8-6887-2008

Odum, J. R., Jungkamp, T. P. W., Griffin, R., Flagan, R. C., & Seinfeld, J. H. (1997). The atmospheric aerosol-forming potential of whole gasoline vapor. *Science*, *276*(5309), 96–99. https://doi.org/10.1126/science.276.5309.96

Parrish, D. D., Ryerson, T. B., Mellqvist, J., Johansson, J., Fried, A., Richter, D., et al. (2012). Primary and secondary sources of formaldehyde in urban atmospheres: Houston Texas region. *Atmospheric Chemistry and Physics*, *12*(7), 3273–3288. https://doi.org/10.5194/acp-12-3273-2012

Rappenglück, B., Lubertino, G., Alvarez, S., Golovko, J., Czader, B., & Ackermann, L. (2013). Radical precursors and related species from traffic as observed and modeled at an urban highway junction. *Journal of the Air & Waste Management Association*, *63*(11), 1270–1286. https://doi.org/10.1080/10962247.2013.822438

Roberts, J. M. (1990). The atmospheric chemistry of organic nitrates. *Atmospheric Environment*, *24A*, 243–287.

Roberts, J. M., Veres, P. R., Cochran, A. K., Warneke, C., Burling, I. R., Yokelson, R. J., et al. (2011). Isocyanic acid in the atmosphere and its possible link to smoke-related health effects. *Proceedings of the National Academy of Sciences of the United States of America*, *108*(22), 8966–8971. https://doi.org/10.1073/pnas.1103352108

Roberts, J. M., Veres, P. R., VandenBoer, T. C., Warneke, C., Graus, M., Williams, E. J., et al. (2014). New insights into atmospheric sources and sinks of isocyanic acid, HNCO, from recent urban and regional observations. *Journal of Geophysical Research: Atmospheres*, *119*, 1060–1072. https://doi.org/10.1002/2013JD019931

Saunders, S. M., Jenkin, M. E., Derwent, R. G., & Pilling, M. J. (2003). Protocol for the development of the Master Chemical Mechanism, MCM v3 (part A): Tropospheric degradation of non-aromatic volatile organic compounds. *Atmospheric Chemistry and Physics*, *3*(1), 161–180. https://doi.org/10.5194/acp-3-161-2003

Schauer, J. J., Kleeman, M. J., Cass, G. R., & Simoneit, B. R. T. (1999). Measurement of emissions from air pollution sources. 2. C1 through C30 organic compounds from medium duty diesel trucks. *Environmental Science & Technology*, *33*(10), 1578–1587. https://doi.org/10.1021/es980081n

Schauer, J. J., Kleeman, M. J., Cass, G. R., & Simoneit, B. R. T. (2002). Measurement of emissions from air pollution sources. 5. C1-C32 organic compounds from gasoline-powered motor vehicles. *Environmental Science & Technology*, *36*(6), 1169–1180. https://doi.org/10.1021/es0108077

Scott, K. I., & Benjamin, M. T. (2003). Development of a biogenic volatile organic compounds emission inventory for the SCOS97-NARSTO domain. *Atmospheric Environment*, *37*, 39–49. https://doi.org/10.1016/S1352-2310(03)00381-9

Sekimoto, K., Inomata, S., Tanimoto, H., Fushimi, A., Fujitani, Y., Sato, K., & Yamada, H. (2013). Characterization of nitromethane emission from automotive exhaust. *Atmospheric Environment*, *81*, 523–531. https://doi.org/10.1016/j.atmosenv.2013.09.031

Shetter, R. E., & Mueller, M. (1999). Photolysis frequency measurements using actinic flux spectroradiometry during the PEM-Tropics mission: Instrumentation description and some results. *Journal of Geophysical Research*, *104*, 5647–5661. https://doi.org/10.1029/98JD01381

Song, Y., Shao, M., Liu, Y., Lu, S., Kuster, W. C., & Goldan, P. D. (2007). Source apportionment of ambient volatile organic compounds in Beijing. *Environmental Science & Technology*, *41*(12), 4348–4353.

Stockwell, W. R., Kirchner, F., & Kuhn, M. (1997). A new mechanism for regional atmospheric chemistry modeling. *Journal of Geophysical Research*, *102*, 25,847–25,879. https://doi.org/10.1029/97JD00849

Szilagyi, I., Dobe, S., Berces, T., Marta, F., & Viskolcz, B. (2004). Direct kinetic study of reactions of hydroxyl radicals with alkyl formates. *Zeitschrift für Physikalische Chemie*, *218*(4-2004), 479–492. https://doi.org/10.1524/zpch.218.4.479.29198

Teruel, M. A., Blanco, M. B., & Luque, G. R. (2007). Atmospheric fate of acrylic acid and acrylonitrile: Rate constants with Cl atoms and OH radicals in the gas phase. *Atmospheric Environment*, *41*(27), 5769–5777. https://doi.org/10.1016/j.atmosenv.2007.02.028

Thalman, R., & Volkamer, R. (2010). Inherent calibration of a blue LED-CE-DOAS instrument to measure iodine oxide, glyoxal, methyl glyoxal, nitrogen dioxide, water vapour and aerosol extinction in open cavity mode. *Atmospheric Measurement Techniques*, *3*(6), 1797–1814. https://doi.org/10.5194/amt-3-1797-2010

Tsai, C., Wong, C., Hurlock, S., Pikelnaya, O., Mielke, L. H., Osthoff, H. D., et al. (2014). Nocturnal loss of NOx during the 2010 CalNex-LA study in the Los Angeles Basin. *Journal of Geophysical Research: Atmospheres*, *119*(22), 13,004–13,025. https://doi.org/10.1002/2014JD022171

Veres, P. R., Roberts, J. M., Cochran, A. K., Gilman, J. B., Kuster, W. C., Holloway, J. S., et al. (2011). Evidence of rapid production of organic acids in an urban air mass. *Geophysical Research Letters*, *38*, L17807. https://doi.org/10.1029/2011GL048420

Veres, P. R., Roberts, J. M., Warneke, C., Welsh-Bon, D., Zahniser, M., Herndon, S., et al. (2008). Development of negative-ion proton-transfer chemical-ionization mass spectrometry (NI-PT-CIMS) for the measurement of gas-phase organic acids in the atmosphere. *International Journal of Mass Spectrometry*, *274*(1-3), 48–55. https://doi.org/10.1016/j.ijms.2008.04.032

Warneke, C., de Gouw, J. A., Edwards, P. M., Holloway, J. S., Gilman, J. B., Kuster, W. C., et al. (2013). Photochemical aging of volatile organic compounds in the Los Angeles basin: Weekday-weekend effect. *Journal of Geophysical Research: Atmospheres*, *118*, 5018–5028. https://doi.org/10.1002/jgrd.50423

Warneke, C., de Gouw, J. A., Lovejoy, E. R., Murphy, P. C., Kuster, W. C., & Fall, R. (2005). Development of proton-transfer ion trap-mass spectrometry: On-line detection and identification of volatile organic compounds in air. *Journal of the American Society for Mass Spectrometry*, *16*(8), 1316–1324. https://doi.org/10.1016/j.jasms.2005.03.025

Warneke, C., McKeen, S. A., de Gouw, J. A., Goldan, P. D., Kuster, W. C., Holloway, J. S., et al. (2007). Determination of urban volatile organic compound emission ratios and comparison with an emissions database. *Journal of Geophysical Research*, *112*, D10S47. https://doi.org/10.1029/2006JD007930

Warneke, C., Veres, P., Holloway, J. S., Stutz, J., Tsai, C., Alvarez, S., et al. (2011). Airborne formaldehyde measurements using PTR-MS: Calibration, humidity dependence, inter-comparison and initial results. *Atmospheric Measurement Techniques*, *4*(10), 2345–2358. https://doi.org/10.5194/amt-4-2345-2011

Washenfelder, R. A., Young, C. J., Brown, S. S., Angevine, W. M., Atlas, E. L., Blake, D. R., et al. (2011). The glyoxal budget and its contribution to organic aerosol for Los Angeles, California during CalNex 2010. *Journal of Geophysical Research*, *116*, D00V02. https://doi.org/10.1029/2011JD016314

Young, C. J., Washenfelder, R. A., Roberts, J. M., Mielke, L. H., Osthoff, H. D., Tsai, C., et al. (2012). Vertically resolved measurements of nighttime radical reservoirs in Los Angeles and their contribution to the urban radical budget. *Environmental Science & Technology*, *46*(20), 10,965–10,973. https://doi.org/10.1021/es302206a

Yuan, B., Shao, M., de Gouw, J., Parrish, D. D., Lu, S., Wang, M., et al. (2012). Volatile organic compounds (VOCs) in urban air: How chemistry affects the interpretation of positive matrix factorization (PMF) analysis. *Journal of Geophysical Research*, *117*, D24302. https://doi.org/10.1029/2012JD018236

Yuan, B., Veres, P. R., Warneke, C., Roberts, J. M., Gilman, J. B., Koss, A., et al. (2015). Investigation of secondary formation of formic acid: Urban environment vs. oil and gas producing region. *Atmospheric Chemistry and Physics*, *15*(4), 1975–1993. https://doi.org/10.5194/acp-15-1975-2015